

# Integrated Structures from Dissimilar Materials: The Future Belongs to Aluminum–Polymer Joints

Tamas Temesi and Tibor Czigany\*

The spread of integrated structural elements and parts made from low-density materials (for example aluminum and polymers) created a need for joining technologies with which these can be joined. Herein, the most important surface preparation methods and joining processes, with which the surface structure of aluminum can be modified and aluminum and polymer structures can be joined, are reviewed. For both topics, a new classification method is introduced: surface preparation methods are grouped based on the method of creating surface structures, whereas joining technologies are grouped according to heat input and structural changes in the polymer material. Herein, “hot” joining technologies (in which so much heat is formed that the polymer material is melted) are reviewed. This grouping category includes techniques based on friction and induction, ultrasonic and laser welding, and some in situ joining technologies. With these, materials with highly different chemical structures and melting temperatures are joined in fast cycles, in a reliable manner. In the coming years, more integrated structures containing aluminum–polymer joints manufactured with fast, automatable joining techniques (such as ultrasonic and laser welding, in compliance with the requirements of Industry 4.0) will be used throughout the industry.

## 1. Introduction

The joining of dissimilar materials, for example, aluminum alloys and polymers with fast joining methods, has recently received increased attention because an important aim of the vehicle (automobile, aerospace, railway, etc.) industry is to decrease costs both during the manufacturing process and during the lifetime the vehicles. The processing and forming of these materials can be

achieved with less energy input, compared with steel and glass products. By lowering the weight of the vehicle, fuel can be saved, and the amount of emissions can also be decreased. The spread of integrated structural elements and parts made from dissimilar, low-density materials brought up the need for joining technologies with which these can be joined.

The joining technologies with which dissimilar materials can be joined can be classified in several ways. One possible method is to group the joining technologies based on the (physical or chemical) principle of action occurring during the joining process. In this classification method, there are three subcategories: shape-connected joints are based on geometric constraints, force-connected joints are based on friction between two surfaces that are pressed together firmly, whereas material-made joints are based on the formation of primary or secondary chemical bonds between the joined materials. A second possible classification method is based on

the detachability of the joint: in this case, the literature differentiates between joints that can be detached nondestructively and joints that can only be detached by damaging the joined objects.<sup>[1]</sup> In this article, we present a new classification method, which is based on the change in the microscopic and also the macroscopic structure of the polymer material during the joining process (Figure 1). We created two subcategories for a more precise classification: in the subcategory called “hot technologies,” we listed several welding and in situ joining technologies, with which it is possible to join metal and polymer materials together. In all of these joining techniques, the materials are heated so that a bond can be created. This usually requires so much heat that the microstructure and even the macrostructure of the polymer material can change: the crystalline structure can be reformed and the polymer can even reach its melting temperature during the joining process. In the subcategory called “cold technologies,” no substantial change in the micro- or macrostructure of the polymer material occurs during or after the joining process. “Cold technologies” are extensively used currently in the automotive and aerospace industry to form integrated structures and join dissimilar materials together. For example, the passenger cell of the BMW i3 and i8 is made from carbon fiber-reinforced composite elements with a thermoset matrix material, and this is bonded to the mostly aluminum body with adhesives.<sup>[2,3]</sup> Thermoset matrix composites and layered hybrid

T. Temesi, Prof. T. Czigany  
Department of Polymer Engineering  
Faculty of Mechanical Engineering  
Budapest University of Technology and Economics  
Muegyetem rkp. 3, H-1111 Budapest, Hungary  
E-mail: czigany@eik.bme.hu

Prof. T. Czigany  
MTA-BME Research Group for Composite Science and Technology  
Muegyetem rkp. 3, H-1111 Budapest, Hungary

 The ORCID identification number(s) for the author(s) of this article can be found under <https://doi.org/10.1002/adem.202000007>.

© 2020 The Authors. Published by WILEY-VCH Verlag GmbH & Co. KGaA, Weinheim. This is an open access article under the terms of the Creative Commons Attribution License, which permits use, distribution and reproduction in any medium, provided the original work is properly cited.

DOI: 10.1002/adem.202000007

structures of aluminum sheets and cross-linked matrix composites (so-called fiber-metal laminates or FMLs) are used in the aviation industry (for example on the wings near the fuel tanks). These are bolted, riveted, or bonded with an adhesive to the metal shell of the airplane.<sup>[1,4]</sup> However, these technologies are usually slow and require multiple preparatory steps (surface preparation and cleaning, boring into or through components, etc.) to be taken before the joining process can even be started. In other, more productive joining techniques (such as ultrasonic welding and laser welding), the polymer material is heated up so that it can bond to the surface of aluminum. Because of the adhesive nature of this bond, the surface preparation of aluminum is especially important, as the global strength of the joint can be increased by structuring the surface, into which the melted polymer can flow during the joining process.

This Review Article confirms that joints between thermoplastic polymers and aluminum and thermoplastic polymer matrix composites and aluminum have been extensively investigated but little information is available on their industrial application. In the framework of the partly EU-funded project with the title “Development of a Direct Laser Joining of Hybrid Plastic-Metal components for industrial applications (PMJoin),” certain automobile industry companies examined the joinability of thermoplastic polymers and aluminum and thermoplastic matrix composites and aluminum by laser welding and the effect of surface preparation of aluminum before laser welding on the load-bearing capacity of the joints. They made various kinds of test specimens: they laser welded the metal circuit elements of the rear light of a Renault Twingo to the polymer body positioning the light bulbs (earlier, this was done by riveting), they replaced some steel structural elements of car seats with a thermoplastic matrix polymer composite, and they welded a biaxial glass fabric-reinforced polyamide matrix composite-reinforcing element into a car door.<sup>[5]</sup> Metal–polymer-integrated medical appliances, so-called lab-on-a-chip devices, eye and ear implants, prostheses, and microelectromechanical systems (MEMS) also attract a great deal of attention. These are made from thermoplastic polymers and metals with a technology that is ready for mass production.<sup>[6,7]</sup>

The aim of this article is to review and categorize surface preparation and joining technologies with which joints between aluminum and polymer materials can be made in mass production.

## 2. Surface Preparation of Aluminum for Joining

Surface preparation is an important step of joining structures either with adhesives, or with welding techniques, as a properly prepared (cleaned, structured) surface significantly influences the strength and load-bearing capacity of the joint. In the case of adhesive bonding, good wettability of the surfaces and low surface tension of the adhesive are also especially important. When materials with dissimilar microstructures (for example metals and polymers) are joined with welding techniques, only the polymer material is melted, which means that only an adhesive connection forms in the joined interface between the materials.<sup>[8–10]</sup>

An adhesive joint forms between two surfaces that are close enough to each other as a result and sum of physical and chemical interactions. This connection makes it possible for load to be



**Tamas Temesi** earned his master’s degree in 2016 in mechanical engineering at the Budapest University of Technology and Economics (BME). He is currently a Ph.D. student at the Department of Polymer Engineering. He has a background in the joining and welding of polymer structures and in the area of manufacturing metal–polymer hybrid structures using laser welding, which is also the subject of his Ph.D. thesis. He is the author of three publications and seven proceedings.



**Tibor Czigan** is currently a professor at the Department of Polymer Engineering at the Budapest University of Technology and Economics (BME). He received his mechanical engineering master’s degree in 1988 and his Ph.D. in 1997 from BME. He is a full member of the Hungarian Academy of Sciences (MTA) and leader of the MTA-BME Research

Group for Composite Science and Technology. His research focuses on polymer engineering, composite materials, and materials testing. He is the author of more than 250 papers and proceedings with more than 4200 independent citations. His cumulative impact factor is 210 and his h-index is 36.

transferred between the surfaces. There is a total of seven separate theories in the literature interpreting and explaining the possible processes as a result of which an adhesive joint is formed. In reality, however, adhesion is almost always formed as a combination of these processes.<sup>[8–10]</sup> In **Figure 2**, we classified the seven theories with a new method based on the scale of action of the main processes. Next, we will discuss these theories in detail.

The “theory of mechanical connection” explains the creation and strength of adhesive joints with the formation of numerous microsized, shape-connected joints in the surface structure (inside grooves, pores, and surface roughness structures) of the materials, meaning that this theory explains adhesion as a result of microscale and mesoscale processes (**Figure 2**).

If adequate pressure and temperature are present during the welding process when materials with a dissimilar structure (for example, aluminum and polymer) are joined, the polymer material is melted: its viscosity is decreased, and as a result, its wettability is increased; thus, it can fill in the surface roughness of the aluminum. According to this theory, the strength of the adhesive joint formed this way can be raised further by increasing the surface roughness (and thus, the size of the surface where joints can be formed) of the metal part. This phenomenon also increases the effect of other adhesive joining mechanisms that are present. However, above a certain surface roughness, the grooves get so deep that the melted polymer cannot fill them fully, meaning that air bubbles are trapped in the joining interface. These voids act as a potential source of cracks and decrease the strength of the joint.

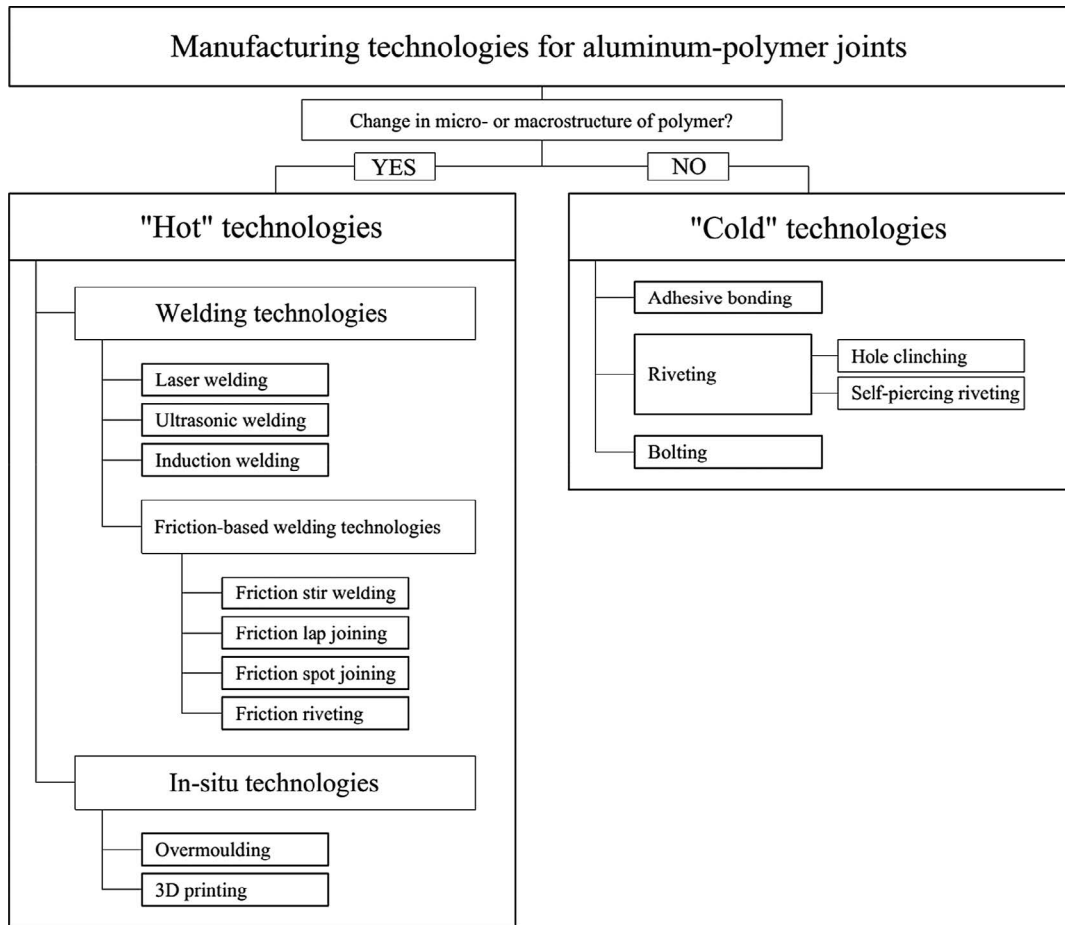


**Figure 1.** New classification method for aluminum–polymer joining technologies.

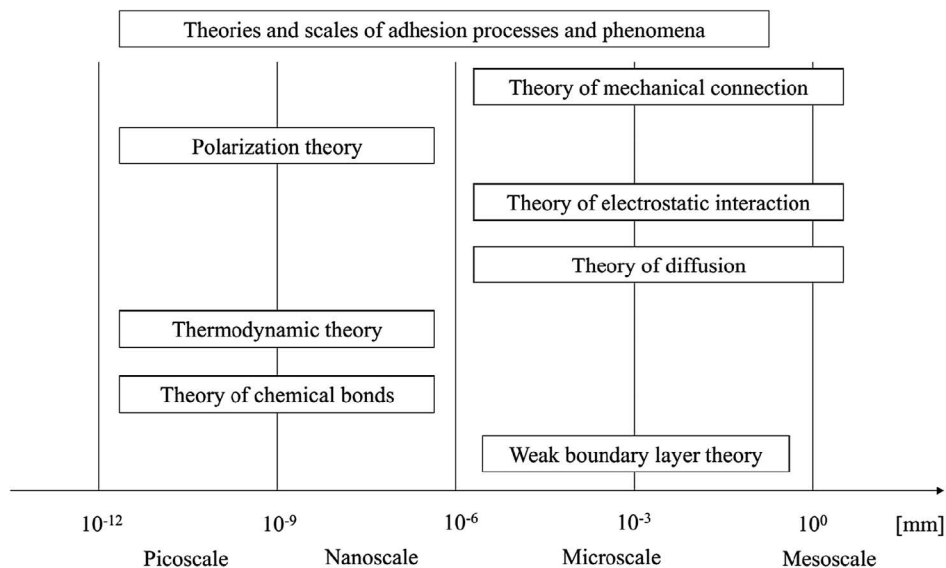


**Figure 2.** Classification of theories of adhesion based on the scale of action.

This theory explains only a part of the phenomenon of adhesion though, as adhesive joints can form between fairly

smooth surfaces where only a fraction of the surface roughness grooves has the proper geometry for strong, shape-connected

joints to form.<sup>[8,9]</sup> In addition to the theory of mechanical connection, there are six more specific theories (based on various phenomena and processes) that explain the formation of adhesive joints. These will be discussed in detail in the following paragraphs.

The “polarization theory” explains adhesion as a result of picoscale and nanoscale phenomena and processes: according to this theory, adhesion is formed between materials that have polar molecules or molecular groups inside them. If these get close enough to each other, a dipole interaction can form between molecules, and furthermore, a hydrogen (secondary) bond can also be created. This theory, however, does not explain adhesion bonds that can form between materials with a nonpolar structure. The “theory of electrostatic interaction” explains the formation of adhesive bonds with microscale and mesoscale processes: electrostatic interaction is based on the difference in electropotential (and thus, charge separation) between the joined materials, if these are close enough to each other. This theory does not explain how or why adhesion works between two samples of the same material. According to the “theory of diffusion,” adhesion forms based on microscale and mesoscale processes when, with adequate temperature and pressure applied, molecules and molecular segments of two, chemically compatible specimens come into contact with each other. This theory on its own does not explain how joints between metal and polymer (or materials with chemically incompatible structures) can be formed. According to the “thermodynamic theory,” good adhesion and great joint strength are based on the wettability of joined materials and influenced by chemical structure and interactions and also the surface energy of the joined materials. This theory states that adhesion is strong if the surface energy of the joined materials is nearly or fully identical and if the materials are constituted by the same type of chemical bond (and thus, the theory explains adhesion with picoscale and nanoscale phenomena and processes). In the case of metal–polymer joints, neither requirement is met; hence, adhesion between these materials is limited based on this theory. According to the “theory of chemical bonds,” adhesion can be greatly increased if covalent (primary chemical) bonds are formed between the joined surfaces. When metal and polymer are joined together, covalent bonds (so-called metal–organic complexes) can form between functional (mainly carbonyl and carboxyl) groups of the polymer and the atoms or the surface oxide layer of the metal. This theory explains adhesion with phenomena and processes on the pico- and nanoscale.<sup>[8–10]</sup>

The “weak boundary layer theory” is usually classified as a specific adhesion theory, although this theory only explains the difference between calculated and measured adhesion forces (the strength of the joint). According to this theory, failure of a joint is preceded by the damage and peeling off of a weak boundary layer inside either material close to the joint interface. This weak layer can be caused by humidity, grease, or other impurities on the surface, by an oxide layer that is loosely connected to the bulk material or by changes in the atomic structure of the materials set on by elevated temperatures during the joining process. Areas rich in additives and/or fillers can also cause a weak boundary layer. This theory explains adhesion with microscale phenomena and processes.<sup>[8–10]</sup>

## 2.1. The Possibilities of Increasing Adhesion

Under normal atmospheric conditions a thin oxide and/or grease and/or water vapor layer always covers the surface of materials; thus, their surfaces must be cleaned and degreased before joining. In metals, the uppermost, thin surface layer always has a different, deformed microstructure compared with the bulk material: it acts as a weak boundary layer, decreasing adhesion. However, this effect can be decreased with a proper surface preparation method.<sup>[11]</sup>

Surface preparation and modification of metals before joining have several beneficial effects: by roughening the surface, a potentially bigger surface can be created for joining (which increases adhesion according to the theory of mechanical connection); by cleaning the surface and removing grease, grime, and water, the chemical composition and structure of the surface can be set and a stable oxide film can be created; and surface tension and the wettability of the surface can also be changed. In the case of polymers, surface modification is usually performed to increase the proportion of active, polar functional groups and the surface energy of the polymer.<sup>[10,11]</sup>

Surface preparation and modification methods are grouped into physical and chemical subcategories by the action principle in the literature, but in this article, we used a novel method for the classification of relevant technologies. We chose the method of creating the surface structure as a basis for categorization: we differentiate between subtractive, additive, and surface-modifying methods (Figure 3).

## 2.2. Subtractive Surface Preparation Methods for Aluminum Specimens

In the case of aluminum–polymer joints, subtractive surface preparation technologies based on a physical action principle are mainly used to create a rougher and thus, a larger surface with more surface structures into which the melted polymer can flow.<sup>[12]</sup> Techniques based on the separation of excess material from the bulk are extensively used in the industry for surface preparation. For aluminum, these technologies are different techniques where different-sized abrasive materials collide with the aluminum at great speed (grit blasting), techniques based on mechanical abrasion to roughen or smoothen the surface of specimens, and technologies based on the microscale or even macroscale manipulation of material on the surface using laser beams (laser ablation, of which an example is shown in Figure 4).<sup>[12–18]</sup>

Anagreh and Al Robaidi<sup>[19]</sup> examined the effect of the process parameters of an arc discharge surface preparation method on the wettability of an aluminum surface and on the shear strength of adhesive-bonded aluminum–thermoset polymer composite specimens. They concluded that the measured increase in the shear strength of the joint was caused by the increased (roughened) surface size and the separation of organic impurities and a magnesium-oxide layer from the surface. Wu et al. used laser ablation (with an Nd:YAG laser) to modify the surface of an AA6022 aluminum alloy before adhesive bonding to the same material. They proved that the impurities can be separated from the surface of aluminum by laser ablation and that with proper laser power, the surface can be roughened, which increased the

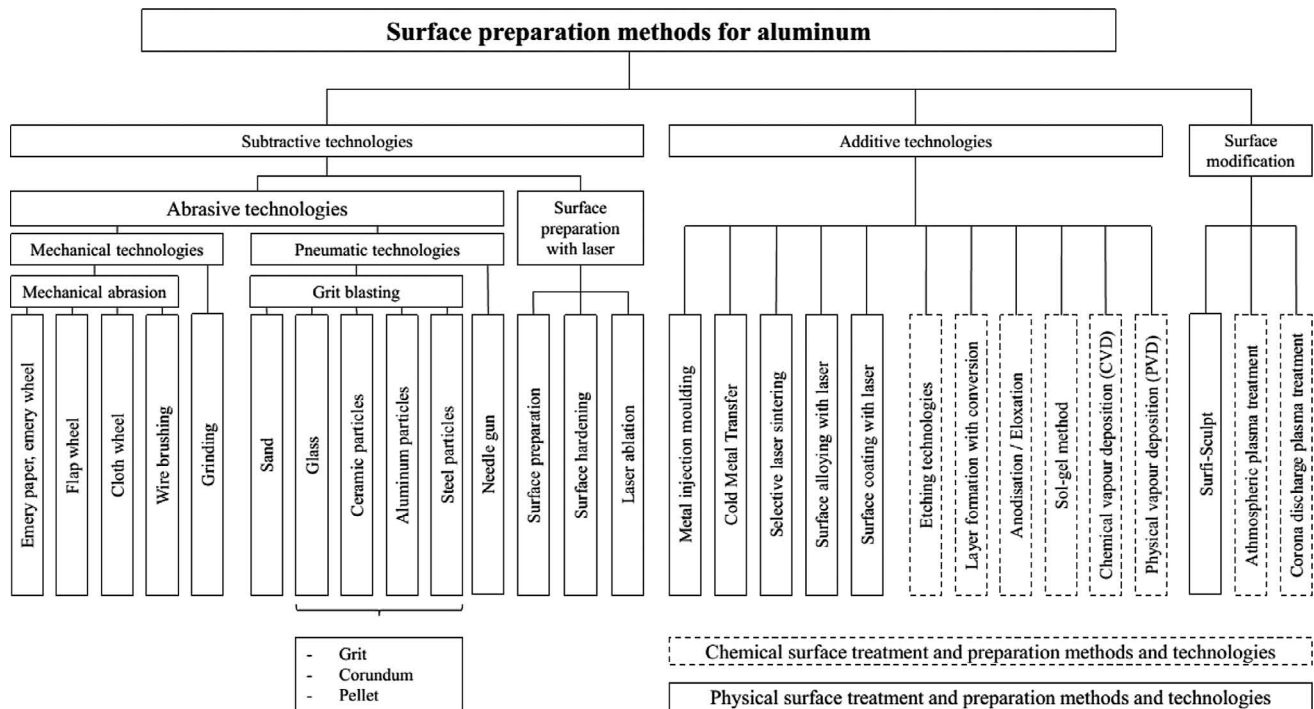


**Figure 3.** Classification of the widely used surface preparation methods for aluminum alloys.

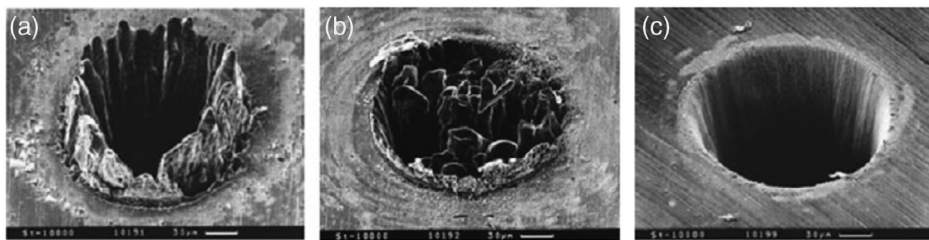


**Figure 4.** Surface preparation of steel in vacuum with a pulsed-mode laser beam. Pulse lengths are a) few nanoseconds, b) picoseconds, and c) femtoseconds, respectively. Reproduced with permission.<sup>[13]</sup> 2014, Springer-Verlag.

shear strength of joints based on the theory of mechanical connection. They also proved with scanning electron microscopy (SEM) and X-ray photoelectron spectroscopy (XPS) analyses that because of the large power density, the laser beam caused chemical and structural changes in the topmost layer of aluminum: the protective oxide layer (which is formed naturally on the surface) thickened and had a more homogeneous structure.<sup>[20]</sup> Kuznetsov et al. examined the wettability of an AlMg6 alloy's surface modified by laser ablation using a pulsed fiber laser. They found that right after the ablation process, the surface of the aluminum became superhydrophilic, the level of which depended on the density of the surface structures, and also showed an exponentially decreasing trend over time (in compliance with the thermodynamic theory).<sup>[21]</sup> Ngo et al. examined the wettability of 99.999% pure aluminum, the surface of which was modified with an Nd:YAG laser: they found that by heat treating the aluminum at 200 °C for 5 h in an oven, its surface became superhydrophobic, whereas treating the aluminum in boiling water for 2 h made its surface superhydrophilic because of the

formation of a nanoscale chemical structure called quasibohemite (AlO(OH)).<sup>[22]</sup> Boehmite, or aluminum hydroxide oxide, can be dispersed well in water, whereas quasibohemite is a hydrophilic material, which can hold a couple of water molecules per AlO(OH) synthesis units and can be used to modify the mechanical properties of thermoplastic polymers and thermoset resins based on the work of Karger-Kocsis and Lendvai<sup>[23]</sup> and Khorasani et al.,<sup>[24]</sup> respectively.

### 2.3. Additive Surface Preparation Methods for Aluminum Specimens

We classified surface preparation technologies into this group that use material from an external source to prepare structures onto the surface of aluminum specimens.

During “metal (powder) injection molding (MIM),” finely ground metal powder blended with easily melted binder materials (for example paraffin or certain types of wax) is processed on a conventional plastic injection molding (IM) machine. After the

molding cycle is complete and the specimens have cooled down properly, the binder material can be melted and released, leaving behind a fragile structure of weakly adhered metal powder frame. This frame then has to be sintered under pressure and at elevated temperatures, during which the frame slightly shrinks in all three dimensions. This technology can be used to manufacture structures with various shapes and sizes on the surface of metal specimens with the so-called overmolding technique.<sup>[25]</sup>

The so-called “cold metal transfer (CMT)” technology is a special variant of the consumable electrode arc welding designed to weld metal structures together. During CMT, the electrode is delivered into the preparation region in a precise manner (a special welding head that can also spool back the electrode when needed is used), so that there is no short circuiting during the process. This way, heat input and the splattering of the consumable electrode can also be decreased.<sup>[26]</sup> CMT is mainly used as a surface preparation method in adhesive bonding and vacuum-assisted resin transfer molding to form penetrative reinforcing pins.<sup>[27–29]</sup>

“Selective laser sintering” or “direct metal laser sintering” (“SLS, DMLS”) is a direct surface preparation technology, in which a finely ground powder (which can even be made from a thermoplastic polymer or a number of metal materials) is melted together with a laser beam layer by layer until the required structure is attained.<sup>[30]</sup>

When aluminum is processed, and highly reactive, pure aluminum gets into contact with atmospheric gases (mainly oxygen), a stable, a few-nanometer-thick surface oxide layer is formed nearly instantaneously. There are some chemical surface modification methods that can be used to further stabilize and thicken this oxide layer. Up until recently, aluminum was widely modified by “chromating”: chrome(III) or chrome(VI) ions were dissolved in an aqueous bath into which the aluminum was submerged. As a result, a stable, corrosion-resistant precipitation layer was formed on the surface. A similar process is called “layer formation with conversion,” during which aluminum is lowered into an acidic or alkaline solution at room temperature or an elevated temperature. During this process, the structure of the natural oxide layer on the surface of the aluminum changes and thickens, forming a resistant surface layer. Due to environmental and health concerns, as chrome is harmful to the environment and some variants (for example chrome(VI)) are toxic, the use of chrome was abandoned (and is now also forbidden), and novel conversion solutions with diverse ion contents (for example, zirconium-based solutions) are intensively searched for and studied.<sup>[12,31]</sup>

Another chemical additive surface preparation method is the so-called “eloxation” process, during which aluminum is connected to the cathode of a direct current power supply and then dipped into an aqueous solution (the anode of the power supply is usually connected to a stainless steel specimen, that remains inert during the eloxation process) containing various electrolytes. As a result of the electrolysis, oxygen atoms become negatively polarized and are torn away from water molecules. These atoms then move towards the cathode, where they encounter elemental aluminum atoms forming a thick, stable surface oxide layer (during electrolysis, the amount of elemental aluminum decreases and hydrogen gas is created). The thickness and surface roughness of this layer depend on the type of electrolyte added to the solution: with sulfuric acid or oxalic acid, the

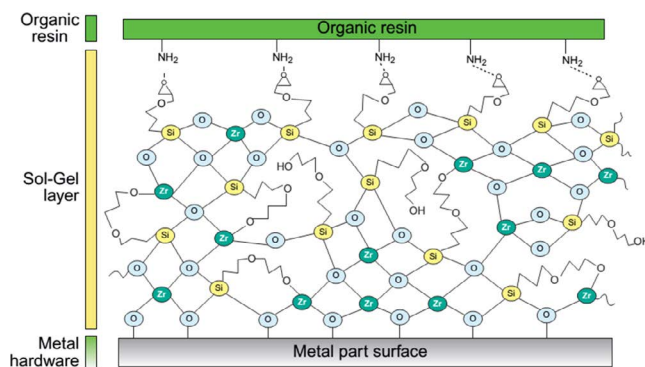


**Figure 5.** Illustration of the working principle of surface modification using the sol-gel method. Reproduced with permission.<sup>[31]</sup> 2013, Elsevier Inc.

thickness of the oxide layer can be set between 30 and 500 micrometers, whereas with phosphoric acid, the surface roughness of the layer can be decreased and a so-called electrochemically polished surface can be created.<sup>[12,31]</sup>

The so-called sol-gel method is used during the adhesive bonding of metals and other, structurally incompatible materials: the sol-gel is a gel-like substance that contains metal oxides and promotes the formation of primary chemical bonds between metal and adhesive (**Figure 5**).<sup>[31]</sup> Other possible additive methods include the physical (PVD) and chemical vapor deposition (CVD) techniques, with which, up until today, only joints formed between glass (with a thin metal layer additively manufactured onto its surface) and thermoplastic polymers were examined.<sup>[32,33]</sup>

#### 2.4. Surface Modification Technologies for Aluminum Specimens

We listed surface preparation technologies in this group that only move material already on the surface of the aluminum specimen to form surface structures (laser beam surface modification), and also those that change certain properties of the atoms and the surface (mainly the wettability) to promote bonding or joining (plasma treatments).

During the so-called Surf-Sculpt process, an electron or laser beam is focused into one point on the surface of the aluminum specimen, where the material is melted and then the energy beam moves away from that spot with mirrors to change the direction of the beam rapidly. Because of the vapor pressure and surface tension, the melted material follows this movement, splattering melted metal and creating surface structures respective to the direction of the movement of the energy beam. In multiple steps and by rotating the energy beam in a circle around the desired point, 2 mm-high pins can be formed, with corresponding grooves around the base of the pins where the material forming the pin was displaced from (**Figure 6**).<sup>[34–36]</sup> This technique is fast and the pins can penetrate the thermoplastic material during the joining of aluminum and polymer materials, forming more shape-connected joints and thus increasing joint strength.<sup>[37–39]</sup>

During plasma treatment, a stream of positively and negatively charged ions, radicals, excited particles, electrons, and photons is created and then contacted with the treated solid surface. Without melting the material on the surface, a number of properties can be

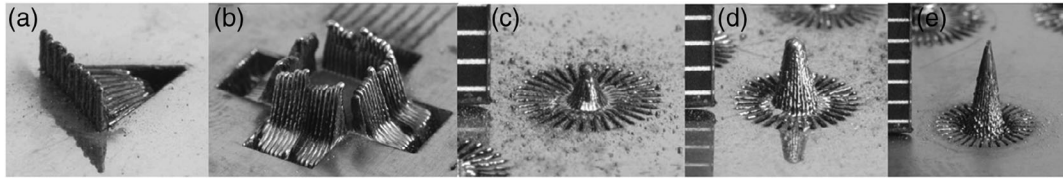


**Figure 6.** Surface structures made with different process control parameters on different metal substrates using the Surf-Sculpt technology (a, c, d) nickel alloy, b, d) titanium alloy). Reproduced with permission.<sup>[34]</sup> 2011, Elsevier Inc.

changed (the wettability and adhesion properties, chemical reactivity, biocompatibility of the surface, etc.), and the surface can also be cleaned from grease and grime. Bónová et al. proved with XPS analysis that aluminum hydroxide and boehmite molecules form on the surface of AA3105 and AA1050 aluminum alloys as a result of atmospheric plasma treatment, making the surface more hydrophilic and increasing its wettability.<sup>[40]</sup> Muñoz et al. used plasma treatment with argon as shielding gas on the surface of AA2024-type aluminum alloys and then coated the surface with polymethyl-methacrylate (PMMA). They proved with a standard droplet test that the wettability of the surface increased as a result of plasma treatment, and they also ran an XPS analysis, confirming that  $Al_2O_3$  molecules formed on the surface, which came in contact with the methoxy functional groups of the PMMA, creating a strong, corrosion-resistant ionic bond between the aluminum and the polymer.<sup>[41]</sup>

### 3. Aluminum–Polymer Joining Technologies

In this chapter, we review the related literature and the joining technologies (denoted “hot technologies” in Figure 1) with which joints between aluminum and polymer materials can be created in mass production, with short cycle times (ranging from seconds to minutes depending on the types of materials and the shape of the joint) and automatable machines.

#### 3.1. Joining Technologies Based on Friction

##### 3.1.1. Friction Spot Joining and Friction Riveting

The “friction spot joining” (“FSpJ”) technology, which can be used to weld metals, polymers, and polymer composites is a variant of the friction spot welding technique patented for welding metal structures together. During the FSpJ process, overlapped joints are manufactured with a rotating tool made of hardened steel connected to a hydraulic press (or a similar machine that can enact pressure on the tool and the welded samples). The joining tool consists of three main parts: a clamping ring is used to hold the tool in place and press the joined materials together during the process, whereas the rotating sleeve and pin (these can even rotate independently of each other) generate the frictional heat necessary for the joining of the materials. The tool is always in contact with the metal part during the joining process.<sup>[1]</sup>

In the first step of the joining process, the tool rotates on the surface of the aluminum specimen, generating heat. When the aluminum is softened, the hydraulic press pushes the sleeve into the aluminum specimen, whereas the pin is retracted; thus, the

softened aluminum fills up the void under the pin. In the next step, the sleeve is retracted, and the pin is pushed toward the joint area; thus, the upper surface of the aluminum becomes smooth again, but a nub is formed on the interface of the aluminum and polymer specimens, which forms the joint between the two materials.<sup>[1]</sup>

Advantages of the friction spot joining technology include ease of building and use and there is no need for predrilling holes or surface preparation. This joining technique is environmentally friendly with no harmful materials emitted during joining. Joints can also be repaired and recreated at the same place. Disadvantages of the technology are that only overlapped joints between moderately thick (between ca. 1 and 5 mm) materials can be created. The joints can withstand shear loads but can easily be broken by torsion or peeling loads.<sup>[1]</sup>

Goushegir et al. manufactured joints between aluminum (AA2024-type and AA6181-type alloys) and carbon fabric-reinforced polyphenylene-sulfide (PPS) composites with the friction spot joining technology (Table 1). They measured the effect of the process parameters and the surface modification of aluminum on the shear strength of the joints and the heat generated during the joining process and they also examined the microstructure of the materials in the joint region. They found that sandblasting the surface of the aluminum alloy removed oxide layers, and surface roughness increased with both surface types used (rolled and alclad). They also found that the shear strength of the joints increased by as much as 20% as a direct result of increased wettability caused by surface modification and that increasing the rotational speed and joining time also positively influenced joint strength. In images made with SEM, the authors also found carbon fibers embedded in the surface structures of the aluminum specimens in the joining zone (called “nub” in Figure 7).<sup>[42–45]</sup>

Lambiase et al. manufactured overlapped joints between AA5053-type aluminum alloy and polyvinylchloride (PVC) specimens using the friction spot joining technology. They investigated the effect of tool pressure and joining time on the strength of the joints. They used a 30 W fiber laser to create a grid-like pattern of the surface structures on the aluminum specimens, which positively influenced joint strength based on their measurements.<sup>[46]</sup> Lambiase and Paoletti joined AA5053-type aluminum alloy (its surface was modified with a laser beam technique) and polyetheretherketone (PEEK) specimens, whereas they examined heat generation in the joining area using an infrared camera. They also calculated the energy input and the shear strength of the joints.<sup>[47]</sup> Ogawa et al. joined an AA5182-type aluminum alloy and polypropylene (PP) reinforced with short carbon fibers using the friction spot joining technology. They investigated the effect of joining time on the strength and fatigue

**Table 1.** Materials, surface preparation methods, test parameters, and mechanical properties of joints made with the friction spot joining technology (n. a. = data not available).

Type and thickness of the aluminum component	Type and thickness of polymer component	Surface preparation method	Shear load or shear strength of the joint ([N] or [MPa])	Test parameters	Ref. no.
AA6181 (1 and 1.5 mm)	PPS-CF43 (2.17 mm)	Roughening with emery paper + surface cleaning with acetone	2100–3500 N	Tool rotational speed (1200–1600 min <sup>-1</sup> ) Tool plunge depth (0.75–1.15 mm) Joining time (2–6 s) Joining force (6800–8300 N)	[42]
AA2024 (2 mm)	PPS-CF50 (2.17 mm)	Rolled and alclad aluminum Sandblasting	15–43 MPa	Tool rotational speed (1000–2900 min <sup>-1</sup> ) Tool plunge depth (0.5 and 0.8 mm) Joining time (4–6.8 s) Joining force (6800–13800 N)	[43]
AA2024 (2 mm)	PPS-CF50 (2.17 mm)	Sandblasting + surface cleaning with acetone	1700–2300 N	Tool rotational speed (1900–2900 min <sup>-1</sup> ) Tool plunge depth (0.5–0.8 mm) Joining time (4–8 s) Joining pressure (0.2–0.3 MPa)	[44]
AA2024 (2 mm)	PPS-CF43 (2.17 mm)	Sandblasting + surface cleaning with acetone	2000–3300 N	Tool rotational speed (1900 and 2900 min <sup>-1</sup> ) Joining pressure (0.2 and 0.3 MPa) The effect of an extra layer of pure PPS placed in between the Al and polymer specimens	[45]
AA5053 (2 mm)	PVC (4 mm)	Laser ablation with fiber laser	3.7–16 MPa	Joining time (5–40 s) Joining force (220 and 320 N)	[46]
AA5053 (2 mm)	PEEK (5 mm)	Laser ablation with fiber laser + cleaning in an ultrasonic bath in ethanol	19–47 MPa	Joining time (15–30 s)	[47]
AA5182 (1.2 mm)	PP-CF40 (3 mm)	Anodizing	4000–7500 N	Joining time (2–5 s)	[48]
AA7075 (2 mm)	PPS-CF (2.17 mm)	Sandblasting	2400–4200 N	Joining force (4000–8000 N)	[49]
AA5052 (2 mm)	HDPE (1 mm)	Surface cleaning with acetone	1400–1600 N (shear load) 13800–14200 N (tensile load)	Tool rotational speed (1000–2000 min <sup>-1</sup> ) Three-layer sandwich structure	[50]
AA5052 (2 mm)	HDPE (1 mm)	Surface cleaning with acetone	700–1200 N (shear load) 13600–13800 N (tensile load)	Tool plunge depth (3.2–3.8 mm) Three-layer sandwich structure	[51]
AA5052 (2 mm)	HDPE (1 mm)	Surface cleaning with acetone	1300–1700 N (shear load) 13800–14400 N (tensile load)	Tool plunge speed (2–12 mm min <sup>-1</sup> ) Three-layer sandwich structure	[52]
AA5052 (2 mm)	PP (2 mm)	Plasma-electrolytic oxidation	150–1350 N 50–1400 N	The effect of surface modification (with and without) The effect of surface modification (with and without) Diameter of predrilled hole (ø 0, 3, 4.5 mm)	[53] [54]
AA5052 (2 mm)	PP (2.8 mm)	Sandblasting and anodizing	200–2200 N	The effect of surface modification (sandblasting or anodizing)	[55]
AA6061 (2 mm)	PP (3 mm)	n. a.	30–290 N	Diameter of predrilled hole (ø 0, 3, 4, 5 mm)	[56]
AA7075 (2 mm)	HDPE (5 mm)	n. a.	22–306 MPa	Tool rotational speed (720–1800 min <sup>-1</sup> ) Tool plunge depth (0.05–0.25 mm) Joining time (5–17 s) Diameter of predrilled hole (ø 2–6 mm)	[57]
AA5052 (2 mm)	PP-CF (2 mm)	n. a.	50–330 N	Tool rotational speed (500–2000 min <sup>-1</sup> )	[58]
AA6082 (3 mm)	PP (3 mm)	n. a.	(n. a.) – 13 MPa	Tool rotational speed (700–1100 min <sup>-1</sup> )	[59]

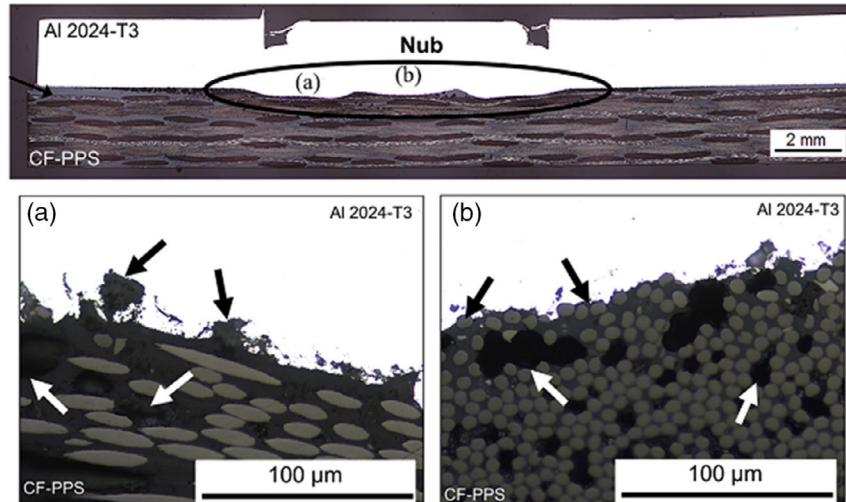


**Figure 7.** Aluminum-carbon fiber-reinforced polymer composite joint made with the friction spot joining technology, a) the polymer filling the surface roughness of the aluminum and b) carbon fibers encompassed by ductile aluminum during joining. Reproduced with permission.<sup>[45]</sup> 2016, Elsevier Inc.

properties of the joints: they found that increasing joining time positively influenced the strength of the joints, because at long joining times, the polymer base material of the thermoplastic composite can be melted more and thus it was able to wet the surface of the aluminum specimen better. With the mechanical fatigue tests, they proved that the propagation of cracks and thus the failure of the joints are mainly influenced by cracks forming near the joining area, in the weak, adhesively bonded layer.<sup>[48]</sup> André et al. joined AA7075-type aluminum alloy and carbon fabric-reinforced PPS specimens together and measured the heat fluctuation in the joining area and the effects of sandblasting (as a surface treatment for aluminum specimens) and tool pressure on the strength of the joints. They also investigated the structure of the joints and the failure modes.<sup>[49]</sup> Rana et al. used a three-layer sandwich structure design when joining AA5052-type aluminum alloy and high-density polyethylene (HDPE) specimens together, using the friction spot joining technology. They investigated the effect of the rotational speed, plunge depth, and plunge speed of the tool on the strength of the joints, the structure of the aluminum specimen, and the structure of the joint itself. They compared the strength of AA-HDPE-AA sandwich structures with the strength of overlapped joints of two aluminum alloy specimens manufactured using the same process control parameters and technique. Their results showed that the tensile strength of the hybrid sandwich structure was greater but the aluminum alloy joints showed superior shear strength,

tensile shear strength, and peeling strength.<sup>[50-52]</sup> Aliasghari et al. joined AA5052-type aluminum alloy and PP specimens together and investigated the effect of surface modification (plasma-electrolytic oxidation of the aluminum alloy) and the effect of predrilled holes in the aluminum specimens on the strength of the joints. Using the plasma-electrolytic oxidation method, they were able to form a porous surface with surface structures in the nanometer range. The melted polymer flowed into these and formed shape-connected joints. When this type of surface modification was used, the strength of the joint was tripled, with the same joining process control parameters and hole diameters.<sup>[53,54]</sup> In a later article, Aliasghari et al. joined the same AA5052-type aluminum and PP specimens together and investigated the effect of sandblasting and anodizing the aluminum specimens on the strength of the joints. They found that the ultimate failure load of the anodized aluminum-PP joints was at least five times higher than the ultimate failure load of the sandblasted aluminum-PP specimens. They attributed this difference to the effect of a porous film layer formed on the surface of aluminum during anodizing, into which the melted PP could flow during the joining process. This film layer is shown in **Figure 8**, where the light-colored part represents the aluminum alloy, the dark part represents the PP material, whereas the grey part is the porous film layer. In the case of anodization, the failure of the joints was mostly caused by ductile failure of the plastic part near the edge of the film layer. In the case of sandblasting,

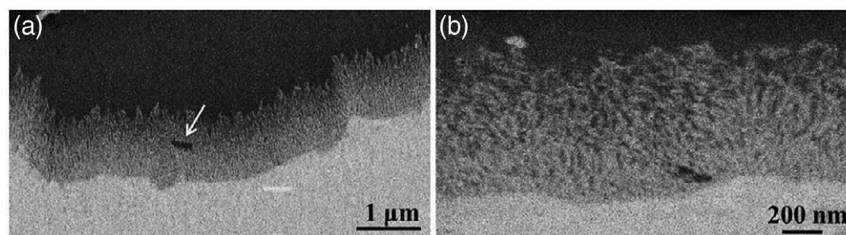


**Figure 8.** a, b) SEM images of micrographs of the aluminum-PP interface in two different magnifications. Reproduced with permission.<sup>[55]</sup> 2019, Elsevier Inc.

the failure of joints was mainly caused by the debonding of the plastic from the aluminum surface at or near the joint interface.<sup>[55]</sup>

In their article, Xiong et al. examined the effect that the diameter of predrilled holes had on the strength of joined AA6061-type aluminum alloy and PP specimens. In SEM images, they found that the joint is unevenly structured, and cracks usually formed on the boundary of the joints. They attributed the latter to the difference in thermal conductivity and thermal expansion between the materials. The authors theorized that the joint was mainly held together by micromechanical interlocking between aluminum and PP and also partly by secondary chemical forces (van der Waals forces). Using differential scanning calorimetry, the authors found that there is no distinct difference in the chemical structure of PP inside and outside the rivet. They also found that increasing the hole diameter increased the mechanical interlocking of aluminum and polymer in the hole, making the joint stronger.<sup>[56]</sup> Abdullah and Hussein joined AA7075-type aluminum alloy and HDPE specimens and examined the effect that the diameter of predrilled holes and changes in tool rotational speed, tool plunge depth, and joining time had on the strength of the joint. They also calculated the heat generated in the joining zone with a finite-element analysis method (FEM) and validated their FEM model using measured values. Based on their findings, heat generation was mainly influenced by tool plunge depth and they got the greatest shear strength with the smallest hole diameters. Joint strength was also highly influenced by the conicity of the holes and the amount of aluminum particles that got into the melted polymer during the joining process.<sup>[57]</sup>

Pabandi et al. modified the friction spot joining technology by drilling a threaded hole in the AA7075-type aluminum alloy before joining it with short carbon fiber-reinforced PP specimens. Strong joints were formed when the melted polymer filled the threaded holes. They found that the strength of these joints was influenced by two parameters: the formation of chemical bonds on the aluminum–polymer interface and the amount of shape-connected

joints that formed in the threaded holes.<sup>[58]</sup> Huang et al. further modified the FSPJ technology by adding a plastic rivet made of PP to the end of the rotating tool when they joined AA6082-type aluminum alloy and PP specimens. These rivets melted while the tool rotated inside the predrilled holes and formed cohesive joints with the PP and adhesive and shape-connected joints with the aluminum specimens as a result.<sup>[59]</sup>

“Friction riveting” is a joining technology patented as a joining method that can be used in the vehicle industry by Amancio-Filho et al.<sup>[1,60]</sup> With this technology, metal rivets or rods can be joined with polymer specimens (**Figure 9a**). The rod or rivet is rotated at a high speed (**Figure 9b**), whereas it is also pressed into the polymer sheet, where heat is generated by friction: both materials heat up, soften, and deform during this step (**Figure 9c**). Because of the pressure on the metal rod, it plastically deforms and forms a pin-like structure and a shape-connected joint inside the polymer material (**Figure 9d**).

The advantages of this technology are that specimens do not require any surface preparation before joining; access is only needed from one side to the specimens; the technology is automatable and cheap to implement. Disadvantages include the fact that depending on the diameter on the metal rod, a certain thickness is required for the polymer specimen; the polymer material can degrade if an excessive amount of heat is generated, and this type of joint concentrates strain into a point.<sup>[1]</sup>

Rodrigues et al. manufactured friction-riveted joints using AA2024-type aluminum alloy rods with a diameter of 5 mm and polycarbonate (PC) specimens, examining the amount of heat generated during the process, and then investigated the mechanical strength and microstructure of the joints (see **Table 2**). They found that the aluminum rods underwent a process called partial dynamic recrystallization because of torque and friction. However, temperatures measured during the joining process did not exceed 360 °C, which is lower than the melting point of the aluminum alloy. They also proved that the hardness of the PC specimens slightly decreased as a result of

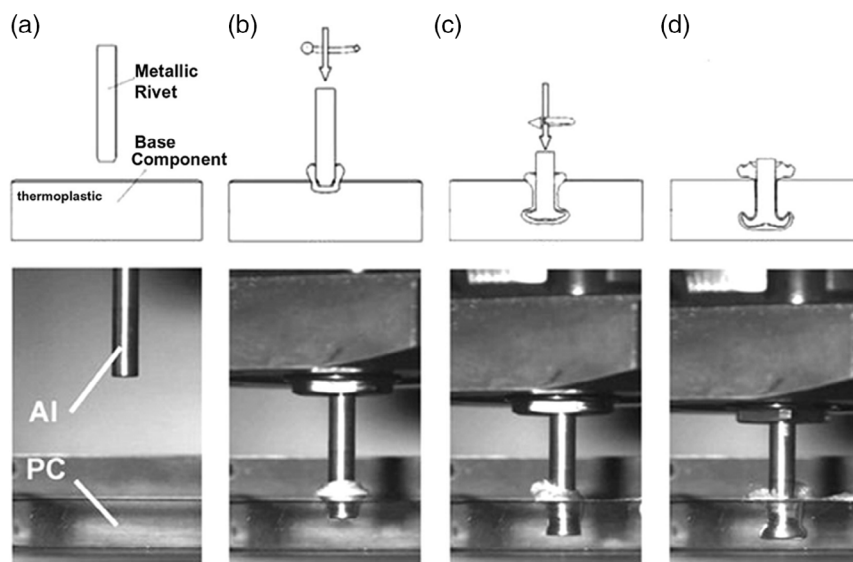


**Figure 9.** Manufacturing a joint between aluminum and PC with the friction riveting technology. a) start of the process, b) the polymer melts in the vicinity of the revolving rivet, c) the rivet is plasticized and deformed, and d) the joining process is complete. Reproduced with permission.<sup>[61]</sup> 2015, Elsevier Inc.

**Table 2.** Materials, test parameters, and mechanical properties of joints made with the friction riveting joining technology.

Type and thickness of aluminum component	Type and thickness of polymer component	Type of rivet	Shear load or shear strength of joint ([N] or [MPa])	Test parameters	Ref. no.
AA2024	PC (15 mm)	Aluminum rod ( $\varnothing$ 5 mm)	6600–8500 N	Rotational speed of rivet (18000–21000 min <sup>-1</sup> ) Riveting pressure (0.75–1.1 MPa) Joining time (3–4 s)	[62]
AA6111 (0.9 mm)	PA6-CF30 (3 mm)	Steel blind rivet	100–3400 N	Rotational speed of rivet (3000–9000 min <sup>-1</sup> ) Riveting speed (60–600 mm min <sup>-1</sup> ) Overlap structure (carbon fiber-reinforced plastic above or below)	[63]

the joining process: the authors theorized that although they did not reach the temperature limit for the degradation of PC, its average molecular weight decreased anyway.<sup>[62]</sup> Min et al. used a so-called blind rivet made of steel to join AA6111-type aluminum alloy and short carbon fiber-reinforced PA6.6 composite specimens together, using the friction riveting technology. They found that the stiffness of the materials to be joined has a great influence on the effectiveness of the joining process and that a thin boundary layer always broke off the composite specimens during joining. This was a weak region in the joined structure during mechanical tests: the damaged areas acted as stress concentration points and greatly contributed to the failure of the joints.<sup>[63]</sup>

### 3.1.2. Friction Lap Joining and Friction Stir Welding

During the so-called “friction lap joining” technology, a rotating tool is pressed onto (also slightly into) the surface of the metal specimen while it also moves along a path. Heat is generated by friction between the tool and the metal specimen (**Figure 10**). In the case of aluminum–polymer joints, the aluminum specimen conducts the heat and transfers it to the polymer specimen, which is melted and thus it can wet the surface of the aluminum, forming shape-connected joints. The rotating tool never contacts the polymer in this joining process. The strength of the joint is further influenced by the pressure with which the rotating tool is pressed onto the surface of the aluminum.<sup>[20]</sup>

Advantages of this joining technology are that it is automatable, cheap to assemble and use, and does not need any extra added material during joining. Disadvantages are that the tool leaves a mark along the path it runs through and that the metal

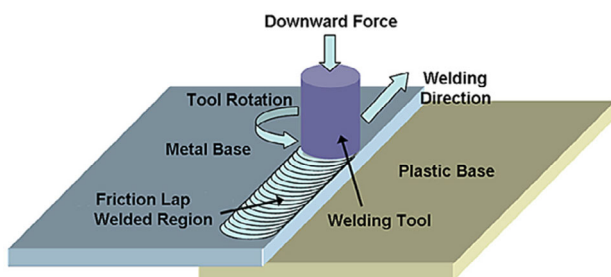


**Figure 10.** Schematic describing the friction lap joining technology. Reproduced with permission.<sup>[64]</sup> 2014, Elsevier Inc.

specimen is under significant mechanical stress during the joining process.<sup>[20]</sup>

Fuchs et al. manufactured joints between AA6082-type aluminum alloy and short glass fiber-reinforced polyamide 6 (PA6) specimens with a constant tool rotation speed, feed rate, and tool pressure (see **Table 3**). They used two surface preparation methods to modify the surface structures of the aluminum specimens: using a 3 kW fiber laser, they manufactured microscopic surface structures, whereas with the Surfi-Sculpt technique, they manufactured microscopic pins. Based on their findings, Surfi-Sculpted pins positively influenced joint strength, because more shape-connected joints and undercuts formed, whereas using the aluminum specimens with the microscopic surface structures, they were able to manufacture joints that had 25% greater strength compared with joints in their literature review.<sup>[37]</sup> Liu et al. manufactured joints between AA6061-type aluminum alloy and PA6 specimens with different tool rotation speeds and feed rates, measured the shear strength of the joints, and examined the structure of the joints. They found a correlation between the layer thickness of the melted PA6, shear strength, and process control parameters: using slower tool rotation speeds and feed rates resulted in less PA6 being melted and a lower shear strength of the joint.<sup>[64]</sup> Nagatsuka et al. manufactured joints between AA5052-type aluminum alloy and short carbon fiber-reinforced PA6 composite specimens using different feed rates. They evaluated the effect of the surface preparation of the aluminum on joint strength. For surface preparation, they used a P800-type emery paper to grind the surface of the aluminum specimens. As a comparison, they used aluminum specimens with their surfaces in an “as-received” (factory-rolled) state. Using the same process control parameters, they found that surface roughening had a significant effect on joint strength: specimens with ground surfaces were able to withstand loads about three times greater than specimens with the “as-received” surface. The joints failed mostly with adhesive-type failure (debonding along the joint surface), whereas in some cases, the composite specimens failed cohesively.<sup>[65]</sup> Bang et al. manufactured joints between AA5052-type aluminum alloy and carbon fabric-reinforced PA6.6 composite specimens using tools with various geometries. They examined the effect of different feed rates and tool plunge depths on the strength of the joints. They found that joints manufactured with the tool with the simplest geometry and smooth surface had the greatest strength, as this could properly melt the PA6.6 matrix material of the

**Table 3.** Materials, surface preparation methods, test parameters, and mechanical properties of joints made with the friction lap joining and the friction stir welding technology (n. a. = data not available).

Type and thickness of aluminum component	Type and thickness of polymer component	Surface preparation method	Shear load or shear strength of joint ([N] or [MPa])	Test parameters	Ref. no.
AA6082 (2 mm)	PA6-GF15 (3 mm) PA6-GF30 (5 mm)	Surfi-Sculpt Laser ablation with fiber laser	5–14 MPa 4–12.5 MPa	Joining force (1500–2000 N) Height of pins formed with Surfi-Sculpt (1.2–2.8 mm)	[37]
AA6061 (2 mm)	PA6 (2 mm)	n. a.	5–8 MPa	Tool diameter (15 and 20 mm) Tool rotational speed (1000–3000 min <sup>-1</sup> ) Feed rate (200–1500 mm min <sup>-1</sup> )	[64]
AA5052 (2 mm)	PA6-CF20 (3 mm)	Roughening with emery paper	1000–3000 N	Feed rate (100–2000 mm min <sup>-1</sup> ) Effect of surface preparation	[65]
AA5052 (1 and 2.5 mm)	PA6-CF (1.5 mm)	Wet polishing	(n. a.) – 8 MPa	Effect of tool design Tool plunge depth (0.8–1 mm) Feed rate (0.6–1 mm s <sup>-1</sup> )	[66,67]
AA6061 (2 mm)	PA6.6 (2 mm)	Depositing thin Al layer with vapor deposition	(n. a.) – 1100 N	Tool rotational speed (800 and 3000 min <sup>-1</sup> ) Feed rate (1–5 m min <sup>-1</sup> ) Thickness of aluminum layer on the polymer (0.8; 1.5; 3.2 nm)	[68,69]
AA5059 (4 mm)	HDPE (4 mm)	n. a.	10 MPa	Tool rotational speed (400–2000 min <sup>-1</sup> ) Feed rate (40–200 mm min <sup>-1</sup> )	[70,71]
AA7075 (3 mm)	PC (3 mm)	n. a.	250–590 N	Tool rotational speed (3000–3500 min <sup>-1</sup> ) Feed rate (50–150 mm min <sup>-1</sup> )	[72]
AA5052 (2 mm)	PP (2.5 mm)	n. a.	2–5 MPa	Tool rotational speed (800–1200 min <sup>-1</sup> )	[73]
AA6061 (3 mm)	PC (3 mm)	n. a.	5–15 MPa	Tool rotational speed (500–1400 min <sup>-1</sup> ) Feed rate (40–80 mm min <sup>-1</sup> )	[74]
AA6111 (1.5 mm)	PPS (2 mm)	Cleaning the surface with ethanol	925–1150 N	Feed rate (10–25 mm min <sup>-1</sup> ) Tool plunge depth (3–3.1 mm)	[75]
AA5058 (4 mm)	PMMA (4 mm)	n. a.	24–45 MPa	Tool plunge depth (0.1–0.4 mm) Tool inclination (0°–2°)	[76]
AA5058 (4 mm)	PMMA (4 mm)	n. a.	28–45 MPa	Tool rotational speed (1250 and 1600 min <sup>-1</sup> ) Feed rate (25 and 50 mm min <sup>-1</sup> )	[77]
AA5754 (4 mm)	PMMA (4 mm)	n. a.	30–50 MPa	Tool rotational speed (750–1730 min <sup>-1</sup> ) Feed rate (60 and 90 mm min <sup>-1</sup> ) Tool inclination (1°–4°) Tool plunge depth (0.2–1.2 mm)	[78]
AA5058 (3 mm)	PC (3 mm)	n. a.	30–45.5 MPa	Tool rotational speed (960–1940 min <sup>-1</sup> ) Feed rate (45 and 90 mm min <sup>-1</sup> )	[79]
AA6061 (2.5 mm)	PEEK (7 mm)	n. a.	14–20 MPa	Feed rate (30–90 mm min <sup>-1</sup> )	[80]
AA2060 (2 mm)	PEEK-CF (3 mm)	n. a.	10–34 MPa	Tool rotational speed (1400–2000 min <sup>-1</sup> ) Tool design	[81,82]
AA6063 (6 mm)	PP (6 mm)	n. a.	0.2–1 MPa	Tool rotational speed (400–1000 min <sup>-1</sup> ) Feed rate (15–50 mm min <sup>-1</sup> )	[83]

composite without damaging the structure of the reinforcing fabric. They also found that smoothening the surface of the aluminum produced joints with greater strength, because polishing the surface resulted in shallower but more structures, into which the melted polymer could flow. The authors also created a numerical model approximating the temperature, which they

validated with real temperature values measured during the joining process.<sup>[66,67]</sup> Liu et al. manufactured a thin Al layer (with thickness in the nanometer range) on the surface of PA6 specimens using the PVD technique before joining it with AA6061-type aluminum alloy specimens. They measured the effect of different tool rotation speeds and feed rates on the

strength of the joints. Using XPS, they found that the Al—O—C chemical bonds formed between the atoms of the aluminum and the carbon atoms located in the polymer chain had a significant effect on the macroscopic strength of the joint.<sup>[68,69]</sup>

During “friction stir welding” (FSW), a rotating tool is pressed and plunged into materials to join them together by stirring melted parts of one specimen into the other and vice versa. Materials are melted by the frictional heat formed on the interface of the rotating tool and the materials themselves (Figure 11).<sup>[84]</sup>

Advantages of this joining technology include ease of use. The process is cheap, automatable, and does not require any additional material to join specimens together. Disadvantages are that only thin parts (with thickness mostly below 10 mm) can be joined in a relatively slow process; the seams also usually contain air bubbles or voids that decrease the strength of the joints.<sup>[84]</sup>

FSW was developed to join aluminum specimens in a solid state, without melting them. This technology is widely used in the vehicle industry to join parts of the petrol tank, heat sinks, nose cone of aerospace vehicles, and also structural elements of aerospace and railway vehicles.<sup>[85]</sup> However, this technology can also be used to join metals other than aluminum<sup>[86]</sup> and polymers<sup>[87,88]</sup>. Kiss and Czigány were amongst the first researchers to prove that FSW can be used to weld polymer specimens together.<sup>[89]</sup>

FSW can also be used to join aluminum and polymer specimens together (Table 3). Khodabakhshi et al. manufactured butt joints between AA5059-type aluminum alloy and HDPE specimens and examined the effect of process control parameters on the aesthetics and mechanical properties of the joints. By investigating the microstructure, they proved that the mechanical properties of the joints are influenced by the adhesion between aluminum and polymer and the formation of micro- and macro-sized undercuts in the joint. They also found that the average strength of the joints was about half of the tensile strength of

the HDPE material they used, whereas the Vickers hardness of the joint was twice the hardness of the HDPE base material.<sup>[70,71]</sup> Moshwan et al. manufactured butt joints between AA7075-type aluminum and PC specimens and examined the tensile strength, the hardness, and the cross section of the joints using two analytical methods (energy-dispersive X-ray spectrometry [EDX] and X-ray diffraction [XRD]). Based on these results, they defined the manufacturing window, with which joints with the greatest strength can be manufactured. They also proved that the hardness of the joint is lower than the hardness of the aluminum base material, which they explained with the presence of voids and air bubbles in the joint and with structural changes of the aluminum as a result of the joining process. They also found that the hardness of the PC decreased near the joint, which they attributed to the thermal degradation of the material. They also proved that no chemical connections formed between the materials, the joint was held together by the undercuts and shape-connected joints.<sup>[72]</sup> Shahmiri et al. manufactured joints between AA5052-type aluminum alloy and PP specimens using a threaded pin as an FSW tool. They found that an interface layer (mainly comprising carbon, oxygen, and aluminum atoms) formed during the FSW process. The thickness of this interface layer depended on heat input: if they decreased feed rate or increased tool rotational speed, the thickness also increased. The global strength of the joint (5 MPa, 20% of the tensile strength of the PP base material) was influenced by this interface layer, as it only weakly, adhesively bonded to both the aluminum and polymer specimens.<sup>[73]</sup> Patel et al. manufactured joints between AA6061-type aluminum alloy and PC specimens. With their measurements, they verified and confirmed the results that Moshwan et al. in a previous study<sup>[72]</sup> had: they did not find a chemical connection between the aluminum and polymer specimens; only undercuts and shapes-connected joints held these joints together. Patel et al. found that the strength of the specimens (15 MPa) they manufactured only reached about third of the tensile strength of the PC base material they used.<sup>[74]</sup> Ratanathavorn and Melander manufactured overlapped joints between AA6111-type aluminum and PPS specimens. During the examination of the macrostructure of the joint, they found that no mixing occurred between the materials and that most of the joint consisted of recrystallized, micro-sized aluminum pieces. They also found a correlation between the size of the pieces and the feed rate. Polymer that melted during the joining process only flowed into gaps between the bulk aluminum and the seam, creating shape-connected joints. They also found air bubbles on the interface between the aluminum and the polymer, the size of which again showed a correlation with feed rate. These air bubbles influenced the failure mode of the joints: when there were many air bubbles, the joints failed by debonding along the interface, whereas in the case of fewer air bubbles, cohesive failure of the PPS material was the prominent failure mode.<sup>[75]</sup> Derazkola et al. manufactured overlapped joints between AA5058-type aluminum alloy and PMMA specimens. They examined the effect of tool tilting angle (in the 0°–2° range), tool plunge depth, tool rotational speed, and feed rate on the strength of the joints. They found micro- and macrosized shape-connected joints between the aluminum and polymer materials. By tilting the FSW tool, or by increasing tool rotational speed, they were able to manufacture joints with high tensile

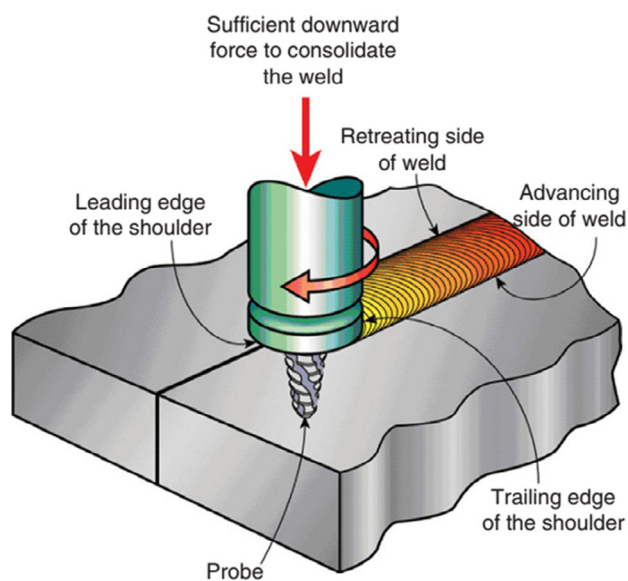


**Figure 11.** Schematic drawing of the friction stir welding joining technology. Reproduced with permission.<sup>[84]</sup> 2009, Elsevier Inc.

strength (45 MPa, about 60% of the tensile strength of the PMMA base material). The authors also created and validated (using the measurement data they acquired) a finite-element model, describing the temperature evolution during the FSW of the materials they used.<sup>[76,77]</sup> In another publication, Derazkola et al. manufactured so-called T-joints between AA5754-type aluminum alloy and PMMA specimens, using a specialized FSW tool. Based on their measurements, enough heat was generated in the joining zone to degrade the PMMA material, and they stated that in addition to the micro- and macro-sized undercuts and shape-connected joints, the chemical connection between the materials also contributed to the strength of the joints.<sup>[78]</sup> In a further article, Derazkola et al. manufactured overlapped joints between AA5058-type aluminum alloy and PC specimens and examined the effect of tool rotation speed and feed rate on the strength (using shear and bending tests) and microstructure of the joints, on the temperature evolution during the joining process, and on the hardness of the joining zone. They proved that the hardness of the PC material in the joining zone decreased, which they explained with the thermal degradation of the polymer during the joining process. They found regions where aluminum anchors formed when they inspected the cross sections taken from the seam. These anchors penetrated the PC material. The shear strength of the joints reached 70%, whereas the bending strength reached 60% of the tensile strength of the PC base material.<sup>[79]</sup> Huang et al. manufactured overlapped joints between AA6061-type aluminum alloy and PEEK specimens using a modified, conical, and triple-faceted FSW tool integrated with a threaded pin. They investigated the effect of tool tilting angle and feed rate on the strength of the joints. They theorized that using the modified tool significantly increases the amount of aluminum embedded into the polymer during the joining process, thus also increasing the number of undercuts and the strength of the joints (max. 20 MPa).<sup>[80]</sup> In later articles, Huang et al. manufactured joints between AA2060-type aluminum alloy and short carbon

fiber-reinforced PEEK specimens using the FSW technique. They examined the effect of tool geometry and tool rotational speed on the shear strength and hardness of the joints. They used a specialized tool with both threaded and tapered surfaces supplemented with a stationary shoulder that was pressed on and smoothed the surface of the seam. They found that aluminum anchors resembling deer antlers penetrated the polymer composite. The failure of the joints occurred by the shearing of these anchors and the debonding of the weak aluminum–polymer interface.<sup>[81,82]</sup> Sahu et al. manufactured joints between AA6063-type aluminum alloy and PP specimens using a cylindrical tool supplemented with a threaded pin, examining the effect of feed rate and tool rotational speeds on the strength of the joints. They found that the strengths of these joints reached only 10% of the tensile strength of the PP base material. They explained this phenomenon with the inadequate mixing of materials during the joining process.<sup>[83]</sup>

### 3.2. Induction and Resistance Welding

Induction welding is mainly used to weld electrically conductive metals together: when such a material is placed into the electromagnetic field generated by a high-frequency alternating current, eddy currents are formed and heat is generated inside the material because of its resistance to the alternating electromagnetic field.<sup>[90]</sup> Metal–polymer and more precisely, aluminum–polymer joints can also be manufactured using this phenomenon (Table 4). There are two main ways in this case: the aluminum can be heated up, which then conducts and transfers heat to the polymer specimen (Figure 12), or it is also possible to heat the polymer if an electrically conductive material (for example carbon fibers) is present inside them.<sup>[96,97]</sup>

Advantages of this joining technology are that it is contactless, cheap, fast, and no additional material is needed to join specimens. The main disadvantage is that only electrically conductive

**Table 4.** Materials, surface preparation methods, test parameters, and mechanical properties of joints made with the induction welding joining technology (n. a. = data not available).

Type and thickness of aluminum component	Type and thickness of polymer component	Surface preparation method	Shear load or shear strength of joint ([N] or [MPa])	Test parameters	Ref. no.
AA5754 (1 mm)	PA6.6–CF48 (2 mm)	Surface cleaning with acetone Grit blasting Chemical preparation methods Plasma cleaning	7–13 MPa	Joining pressure (0.5–3 MPa) Surface preparation Thickness of the polymer interlayer (50–200 μm) Type of carbon fabric (three different types)	[91]
AA5754 (1 mm)	PA6.6–CF48 (2 mm)	Surface cleaning with acetone Grit blasting Chemical preparation methods	7–16 MPa	Surface preparation Cooling rate (22–25 °C s <sup>-1</sup> )	[92]
AA5754 (1 mm)	PA6.6–CF48 (2 mm)	Surface cleaning with acetone Chemical preparation methods	0–14.5 MPa	Surface preparation Aging of aluminum before joining (three methods) Aging of joints in open air (6–12 months)	[93]
AA6016 (1.15 mm)	PA6 PA6–GF47 (2 mm)	Grit blasting Laser ablation with fiber laser	n. a. 2000–4000 N	Surface preparation Joining time (0.2–1.8 s) Amperage (2–17 kA)	[94]

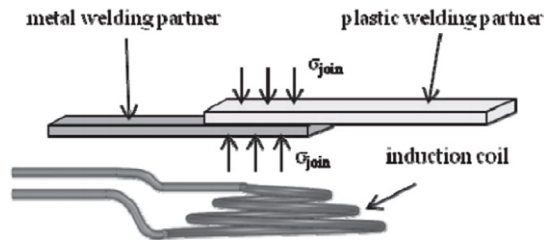


**Figure 12.** Schematic of the induction welding joining technology. Reproduced with permission.<sup>[95]</sup> 2011, Elsevier Inc.

materials can be used; furthermore, there must be enough free space around the specimens for the induction coil.<sup>[1]</sup>

Resistance spot welding is widely used in the industry to weld sheet metal specimens and components together. A welding machine with two clamps is used to press two (or more) metal specimens together, whereas electric current flows through the clamps and the specimens. As the welding current is concentrated into a small area, it can melt thin layers of metal in the vicinity of the clamps. The basic resistance spot welding technique must be modified to use this joining technique to weld metal and polymer materials together (as polymer materials usually do not conduct electricity). Advantages of this joining technology include easy automation, minor process costs, and short welding times. The main disadvantage of the conventional resistance spot welding technique is that it requires access on both sides of the specimens to be welded.<sup>[94]</sup>

Mitschang et al. used an induction welding setup to manufacture overlapped joints between AA5754-type aluminum alloy and carbon fabric-reinforced PA6.6 specimens. They measured the effect of various physical and chemical pretreatment methods and the effect of the resulting surface structures, the effect of joining pressure, the effect of placing additional unreinforced PA6 layers between the aluminum and composite materials, and the effect of temperature generated during the joining process on the shear strength of the manufactured joints. Based on their results, the surface preparation (especially by sandblasting and by acidic pickling) of aluminum and polymer (with corona discharge plasma treatment) significantly increased the shear strength of the joints and decreased the standard deviation of the measured strength values. They also proved that joining pressure had the most effect on the strength of the joints, as it influenced the viscosity of the melted polymer during the joining process. Adding an unreinforced layer of polymer between the aluminum and polymer could also facilitate the manufacturing of strong joints.<sup>[91]</sup> In a later article, Mitschang et al. presented an automatable induction spot welding joining technique that operated with a tempered tool, with which they were able to replicate joints with the same materials as in their previous article. Furthermore, they were also able to join steel and carbon fabric-reinforced PEEK specimens together.<sup>[92]</sup> Didi et al. manufactured joints between AA5754-type aluminum alloy and carbon fabric-reinforced PA6.6 specimens using the induction welding technique. They investigated the effect of different surface preparation methods and open-air aging on the strength of the joints. They proved that the aging of aluminum before joining had a significant negative effect on the shear strength of the joints

except when the aluminum specimens were aged after acidic etching (in this case, the aging process only had a slight effect on joint strength). They also found that during acidic etching, surface structures in the nanoscale formed on the surface of the aluminum. The polymer melt flowed into these easily, forming many shape-connected joints, resulting in a generally stronger joint.<sup>[93]</sup> Szallies et al. used the resistance spot welding technique to manufacture joints between AA6016-type aluminum alloy and PA6 specimens and also long glass fiber-reinforced PA6 specimens. They proved that the resistance spot welding technique, which is already widely used to weld metal specimens together, could also be used to join aluminum and polymer specimens. They investigated the effect of aluminum surface preparation (by sandblasting and laser ablation), joining time and amperage on the strength of the joints. They found that the joined specimens, in which the surface of the aluminum was prepared using laser ablation, had better strength and flexibility.<sup>[94]</sup>

### 3.3. Ultrasonic Welding

Ultrasonic welding is one of the most widely used joining technologies for thermoplastic polymer structures. During ultrasonic welding, the energy necessary to join polymer materials is provided by high-frequency (20–40 kHz), low-amplitude (1–25 μm) mechanical vibrations. These are generated by the ultrasonic welding machine itself when voltage is connected to a piezoelectric crystal: when current runs through this material, it can rapidly contract and expand (the frequency is based on the frequency of the current), generating the vibrations. These are then coupled through the pieces of the welding machine: the converter, the booster, and the horn (also called the sonotrode), which can modify both the amplitude and the frequency of the vibrations. The inherent energy in the mechanical vibrations is converted to heat during the welding process: part of the energy is consumed when bonds between molecules and molecular chains of a polymer break and molecular segments start to slip on and parallel to each other (this is called the macro-Brown movement of polymer chains). The rest of the energy of the vibrations is transformed into heat by friction on the interface between the materials to be joined. This also means that to have an effective joining process, materials must be firmly clamped together; so that heat generation is maximized on the interface of the materials. It is also possible to use ultrasonic welding to join aluminum and polymer specimens (Table 5), but a special sonotrode and clamping structure is needed so that the aluminum does not bond to the metal parts and fixtures in the machine.<sup>[84]</sup>

Advantages of this technology are that welding cycles are fast and automatable. Thus, this technology can easily be used in mass production; joints and seams are strong and solid; no additional material is needed for joining; furthermore, it can be used to embed metal parts into polymer structures and directly join metal and polymer structures. Disadvantages include limitations in seam size and shape, as the maximum seam size in one welding step is not larger than 250 × 300 mm and the prices of tools increase with tool size and the fact that special tooling is needed for the formation of geometrically complex joints.<sup>[1,84]</sup>

Balle et al. manufactured joints between AA1050-type and AA5754-type aluminum alloys and carbon fiber-reinforced

**Table 5.** Materials, surface preparation methods, test parameters, and mechanical properties of joints made with ultrasonic welding (n. a. = data not available).

Type and thickness of aluminum component	Type and thickness of polymer component	Surface preparation method	Ultimate strength of joint [MPa]	Test parameters	Ref. no.
AA1050 (1 mm)	PA6.6–CF48 (2 mm)	n. a.	17–25 MPa	Joining force (55–85 N) Amplitude of vibrations (29–35 $\mu\text{m}$ ) Welding energy (1550–1850 J)	[98,99]
AA5754 (1 mm)			24–31.5 MPa	Joining force (100–220 N) Amplitude of vibrations (37–43 $\mu\text{m}$ ) Welding energy (1700–2300 J)	
AA5754 (1 mm)	PA6.6–CF48 (2 mm)	Grit blasting Etching	35–50 MPa	Welding energy (1800–2200 J) Joining force (120–200 N) Amplitude of vibrations (38–42 $\mu\text{m}$ )	[100]
AA5052 (1.5 mm)	ABS (1.5 mm)	Laser ablation with fiber laser	1.5–11 MPa	Depth of surface structures (170–320 $\mu\text{m}$ ) Groove width (40–100 $\mu\text{m}$ ) Grid width (130–280 $\mu\text{m}$ ) Preheating temperature of aluminum (25–80 °C) Welding time (0.1–0.12 s)	[101]
AA6082 (1 and 1.5 and 2 mm)	ABS (2 mm)	Chemical treatment (ASTM D3933-98)	(n. a.) – 2.3 MPa	Amplitude of vibrations (16.8–21 $\mu\text{m}$ ) Welding time (1–2 s) Joining force (850–1050 N) Shape of energy director (triangular, semicircular, rectangular) Thickness of aluminum (1–2 mm)	[102]
AA6061 (0.9 mm)	PA6–CF50 (2 mm)	<b>Chemical:</b> etching and surface coating (TiZr) <b>Mechanical:</b> Grit blasting, laser ablation, 3D printing, “grip-metal” technology <b>Physical:</b> Plasma cleaning	7–15 MPa	Effects of different surface treatments	[103]
AA2198 (1.2 mm)	PEEK–CF	Cleaning in an ultrasonic bath in ethanol	50–65 MPa 22–41 MPa	Joining force (200–400 N) Welding energy (3500–4600 J)	[104]
AA5024 (1.2 mm)	PPS–CF (1.8 mm)		(n. a.) – 83 MPa (n. a.) – 79 MPa	Amplitude of vibrations (36.5–50 $\mu\text{m}$ ) Heat treatment of AA2198-type specimens	

PA6.6, composite specimens, achieving outstanding shear strength (30 MPa). They also found that there were carbon fibers embedded in the surface roughness ditches, whereas the thermoplastic matrix material of the composite was displaced to the edge of the joining zone. They proved that the technology could also be used to weld structural steel and PA6.6-based thermoplastic composites together.<sup>[98,99]</sup> Wagner et al. used two different aluminum alloys (AA2024 and AA5754) and joined these to short carbon fiber-reinforced PA6.6 composite specimens, reaching a shear strength of 30 MPa. When they also prepared the surface of the AA5754 alloy before joining (using sandblasting and acidic etching), they were able to manufacture joints with a shear strength of 50 MPa.<sup>[100]</sup> Yeh and Hsu joined AA5052-type aluminum alloy (its surface was prepared by laser ablation by a fiber laser) and acrylonitrile–butadiene–styrene (ABS) specimens. They found that the density of structures on the surface (**Figure 13**) has a significant influence on the shear strength and the failure mode of the joints. They proved that heating

up to 60 °C the clamping system that holds the specimens together during welding also had a positive effect on the shear strength of the joints.<sup>[101]</sup>

Al-Obaidi and Majewski manufactured joints between AA6082-type aluminum alloy and ABS specimens using the ultrasonic welding technique. The surfaces of the aluminum specimens were chemically etched, forming a loose, porous surface structure. They examined the effect of the thickness of the aluminum specimen, the amplitude of the vibrations, the joining time, the joining force, and so-called energy directors on the polymer surface on the strength of the joints. They found that preparing the surface of the aluminum is important; without chemical etching, they could not manufacture joints between the materials. Increasing the amplitude of the vibrations led to stronger joints, whereas increasing joining force, joining time, and aluminum thickness all negatively influenced joint strength. In the case of energy directors, the best joint strength was achieved when they used a triangle-shaped structure.<sup>[102]</sup>

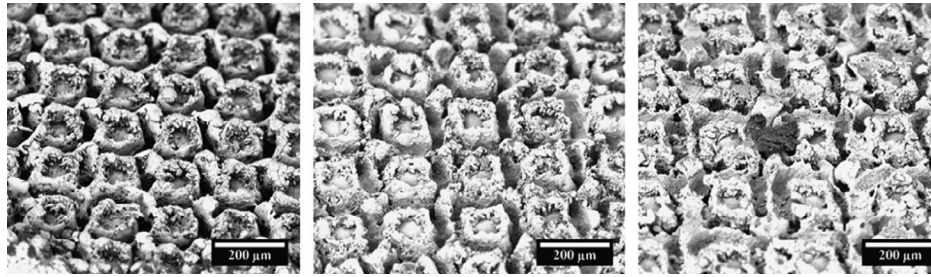


**Figure 13.** The surface of aluminum–ABS specimens after the tensile testing of Al–ABS joints made by ultrasonic welding—the aluminum surfaces were prepared by laser ablation with different process parameters. Reproduced with permission.<sup>[99]</sup> 2016, Elsevier Inc.

Dal Conte et al. manufactured joints between AA6061-type aluminum alloy and carbon fabric-reinforced PA6 composite specimens. They investigated the effect of various surface preparation techniques (see Table 5) on the strength of the joints. They also formed energy directors on the surface of the PA6 specimens by melting a 0.24 mm-thick PA6 foil in a mold under pressure. They examined the wettability of the aluminum surface for each surface preparation technique with the water droplet test. They found that plasma cleaning and TiZr coating resulted in the best wettability, but the strongest joints were created with aluminum specimens with a laser-ablated surface.<sup>[103]</sup> Staab and Balle manufactured joints using the so-called torsion ultrasonic welding technique. They joined specimens from two different aluminum alloys (AA2198 and AA5024) and two different thermoplastic composites (carbon fabric-reinforced PEEK and carbon fabric-reinforced PPS). They also used a specially designed, cylindrical sonotrode. They achieved the greatest joint strength when the AA5024-type alloy and carbon fabric-reinforced PEEK were welded together. The heat treatment of the AA2198-type alloy significantly decreased the standard deviation of shear strength values and increased the load-bearing capacity of the manufactured joints. In the case of the AA5024-type alloy, heat treatment had no effect on joint strength. Below 1.8 s of welding time, only an adhesion-type joint was formed between the specimens, but above this time limit, a friction-based strong joint was formed between aluminum and polymer.<sup>[104]</sup>

### 3.4. Laser Welding

Laser welding is increasingly used as a joining technology for manufacturing metal–polymer joints (in addition to being widely used in the industry to weld, cut, or modify metals and polymers alike). There are multiple laser welding machines that can be used: in the industry, diode lasers, fiber lasers, and Nd:YAG lasers are generally used for welding. Laser beams generated by these machines have a wavelength in the near-infrared spectrum, between 900 and 1100 nm. Publications usually deal with problems related to the leading fields of the industry (vehicle and space engineering, medical technology), and authors usually test the laser weldability of structural materials related to these fields (Table 6).<sup>[39,105,116–121]</sup> Of all possible metallic materials, aluminum, steel, and titanium alloys are extensively used in research. As far as thermoplastic polymers go, researchers use

thermoplastic composites (mainly with polyamide as a matrix material) in about one-third of the publications, with the rest being unreinforced thermoplastic materials ranging from ordinary PP,<sup>[106,122]</sup> polyethylene terephthalate (PET), and PC,<sup>[107,123–131]</sup> to engineering plastics like polyimide (PI) and polyvinylidene fluoride (PVDF).<sup>[39,108,117,132–135]</sup>

Advantages of the laser welding technique in the joining of aluminum–polymer structures are that the process is fast, easily automatable, and contactless; no additional material (like adhesive or additives) is needed to join structures; joints are usually strong and solid, and the size of the joint can be varied freely. Disadvantages include the fact that only thermoplastic polymers and polymer composites can be used and proper fixtures and equipment are needed for pressing the welded specimens together well and without an air gap between them (Figure 14). Also, laser safety precautions for the operators must be taken seriously.<sup>[1,84]</sup>

Gower et al. were among the first researchers to prove that laser welding can be used to join aluminum and polymer specimens, by manufacturing joints between AA5182-type aluminum alloy and PP specimens with both spot welding and linear welding. However, during spot welding, they found that the polymer material degraded and cracked because of the significant localized thermal load.<sup>[106]</sup> Farazila et al. manufactured joints between AA5052-type aluminum alloy and PET specimens using Nd:YAG laser welding machine. They proved that much more energy was needed to create a strong joint between aluminum and PET than between steel and PET. They attributed this to the higher thermal conductivity of the aluminum and the fact that much of the laser beam was reflected off the surface of the aluminum specimen.<sup>[107]</sup>

Yusof et al. manufactured joints using AA5052-type aluminum alloy and PET with the use of Nd:YAG laser and examined the effect of the anodization of aluminum on the strength of the joint. They proved (in accordance with results of Farazila et al. in a previous study<sup>[107]</sup>) that the amount of released heat energy during joining has a significant effect on the shear strength of laser-welded joints. They were able to change heat release rates on the surface of aluminum by anodizing the surface, and they explained this phenomenon with the increased absorption (and thus, decreased reflection) of the laser beam on the surface.<sup>[109]</sup> Zhang et al. manufactured joints between AA6061-type aluminum alloy (with a surface anodized with a solution containing phosphoric acid) and carbon fiber-reinforced PA6 thermoplastic composite specimens with the use of a fiber laser.

**Table 6.** Materials, surface preparation methods, laser welding machine types, test parameters, and mechanical properties of joints made with laser welding (n. a. = data not available).

Type and thickness of aluminum component	Type and thickness of polymer component	Surface preparation method	Type and power of laser welding machine	Shear load or shear strength of joint ([N] or [MPa])	Test parameters	Ref. no.
AA6082 (2 mm)	PA6–GF15	With fiber laser	Diode laser	7.5–24 MPa	Time of formation for surface structures (10–15 s)	[38]
	PA6.6–GF50		$P_w = 250\text{--}500\text{ W}$	7–35 MPa		
	PBT–GF60 (2–4 mm)			11–37 MPa		
AA7050 (2 mm)	PA6–CF22 (3.5 mm)	Surfi-Sculpt	Fiber laser	2–39 MPa	Distance between surface structures (0.5–1.3 mm), repetitions (140–380)	[39]
			$P_w = 1000\text{--}1300\text{ W}$			
AA5052 (1 mm)	PA6–CF20 (3 mm)	Cleaning the surface with ethanol	Diode laser	1000–3000 N	Welding speed (1–5 mm s <sup>-1</sup> )	[105]
			$P_w = 600\text{--}1300\text{ W}$			
AA5182 (0.25 mm)	PP (0.8 mm)	n. a.	Nd:YAG laser	n. a.	Duration of laser pulse (1–10 ms)	[106]
			$P_w = 300\text{--}1000\text{ W}$			
AA5052 (1 mm)	PET (0.5 mm)	Cleaning the surface with acetone and ethanol	Nd:YAG laser (pulsed mode)	0.1–4.5 MPa	Duration of laser pulse (5–20 ms); Energy input with each impulse (14–65 J impulse <sup>-1</sup> );	[107]
AA5182 (1.2 mm)	PC	With Nd:YAG laser + infrared heating ( $P_{IR}$ : 150 W)	$P_{laser}$ : 60 W;	5.7–19.7 MPa	Surface structures' depth of grid pattern (160–200 μm), depth of hole pattern (200–450 μm)	[108]
	PA6		$P_{laser}$ : 45 W;	7.8–16.3 MPa		
	PA6–GF30 (2 mm)		$P_{laser}$ : 70 W	7.7–20.8 MPa		
			Diode laser			
AA5052 (1 mm)	PET (0.5 mm)	Anodizing	Nd:YAG laser (pulsed mode)	2–8 MPa	Duration of laser pulse (5–20 ms); Energy input (5.9–55.8 J);	[109]
AA6061 (2 mm)	PA6–CF22 (3.5 mm)	Anodizing + cleaning the surface with ethanol	Fiber laser	5–41.8 MPa	Anodizing time (10 and 30 min)	[110]
			$P_w = 800\text{--}2000\text{ W}$			
AA1050 (0.5 mm)	PA6.6 (1 mm)	Anodizing and laser ablation	Fiber laser	600–1600 N	Depth of surface roughness (0.14–1.12 μm)	[111]
			$P_w = 210\text{--}350\text{ W}$			
AA5053 (2 mm)	PEEK (5 mm)	With fiber laser	Diode laser	10–30 MPa	Energy of laser beam (2000–4000 J)	[112]
			$P_w = 100\text{--}200\text{ W}$			
AA5053 (2 mm)	PVC (3 mm)	With fiber laser	Diode laser	0.1–15 MPa	Speed of surface preparation (25–150 mm min <sup>-1</sup> )	[113]
			$P_w = 100\text{--}200\text{ W}$			
AA6082 (1.5 mm)	PA6.6 (2 mm)	With fiber laser	Diode laser	2600–7300 N	Welding speed (2–7 mm s <sup>-1</sup> )	[114]
			$P_w = 1000\text{ W}$		Open-air aging	
					Effect of heat treatment	
AA1050 (0.5 mm)	PA6.6 (4 mm)	With Nd:YVO <sub>4</sub> laser	Fiber laser	900–1465 N	Effect of multiple surface preparation parameters	[115]
			$P_w = 400\text{ W}$			

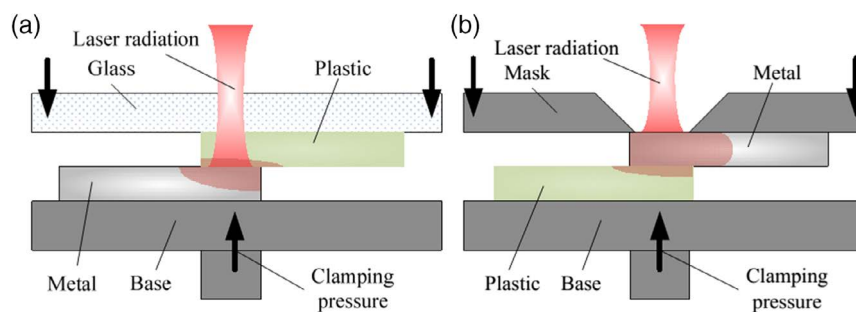


**Figure 14.** Schematic of the a) transmission laser welding and b) the direct laser welding technologies used to join metal and polymer specimens together. Reproduced with permission.<sup>[38]</sup> 2014, Elsevier Inc.

They examined the effect of anodization time on the shear strength of the joints and using SEM, they found that a porous layer formed on the surface of aluminum with the size of the pores depending on anodization time. When anodization lasted for more than 30 min, pores were big and the layer had a loose texture with low adhesion to the bulk aluminum. They explained this phenomenon with the highly corrosive nature of phosphoric acid. They also investigated how the average value of surface roughness changed as a result of the surface preparation method: the authors found that increased anodization time resulted in a smoother surface. Thus, less shape-connected joints formed and joints became weaker when the anodization time increased (in accordance with their measurement results). Using an XPS machine, they also found that the unsaturated double bond in the carbonyl group of the PA6 matrix material dissociated during the joining process, and the highly reactive oxygen atom that formed was able to form a primary chemical bond with positively charged aluminum atoms in the oxide layer of the aluminum specimen. Based on these observations, Zhang et al. concluded that the shear strength of aluminum-PA6/CF joints depends on the surface roughness and the primary chemical bonds formed during the joining process, the amount of which can be manipulated with the anodization process.<sup>[110]</sup> Amend et al. manufactured joints between AA5182-type aluminum alloy and PC specimens using a diode laser. They also manufactured joints between the same AA5182-type aluminum alloy and PA6 and also glass fiber-reinforced PA6 thermoplastic composite specimens using a diode laser and an infrared energy source emitting polychromatic radiation (to heat the joined specimens further). The surface of the aluminum specimens was prepared with an Nd:YAG laser in two ways: in one method, the authors created semicircular holes in the surface, whereas in the other method, a grid-like pattern was formed. In addition to evaluating the effect of these surface structures on joint strength, the authors also conducted shear tests in accordance with BMW's specific standard, PR308.2. Tests based on this standard test the long-term performance of overlapped joints after a thermal aging cycle (in this article, the authors conducted thermal aging in 20 cycles, with varying humidity levels and temperature limits ranging from  $-40$  to  $120$  °C in a single cycle). In case of the PC specimens, the authors used transmission welding, whereas with polyamide-based materials, they used direct laser welding to manufacture joints (see Figure 14 for further reference). The standard deviation of the aluminum-PC joints was high, but an average shear strength of 16 MPa (with semicircular holes) and 20 MPa (with the grid-like structure) was attained. For PA6-based polymers, joints between aluminum (with grid-like structures) and polymer were manufactured only: the authors presented average shear strength values of 15 MPa for aluminum-PA6 and 20 MPa for aluminum-PA6/GF joints. They also found that the failure of the joints always occurred with the cohesive failure of the polymer far away from the joining area. When thermal aging was used, the shear strength of the measured joints declined.<sup>[108]</sup> Jung et al. manufactured joints between AA5052-type aluminum alloy and long carbon fiber-reinforced PA6 composite specimens using a diode laser and an inert nitrogen shielding gas. During the shear test of the joints, they found that joints also formed between the aluminum and the carbon fibers. Using a transmission electron microscope, they proved that this joint is in fact

formed between the carbon fibers and a thin (nanometer-wide)  $\kappa$ - $\text{Al}_2\text{O}_3$  layer on the surface of the aluminum specimen.<sup>[105]</sup> Lamberti et al. manufactured joints between AA1050-type aluminum alloy and PA6.6 specimens using a fiber laser. They modified the surface structure of the aluminum specimens using two different methods: with a pulsed laser beam, they roughened the surface, while using anodization, and they reduced the roughness of the surface. They found that both methods had a significant effect on the shear strength of the joints. Using Fourier-transform infrared spectroscopy (FTIR), they also found that an increase in shear strength was due to the formation of secondary hydrogen bonds between the materials on the joining interface.<sup>[111]</sup>

Heckert and Zaeh used a diode laser and the direct laser joining technique to manufacture joints between AA6082-type aluminum alloy and multiple thermoplastic composites: the authors used short glass fiber-reinforced PA6 (PA6/GF15), long glass fiber-reinforced PA6 (PA6/GF50), and unidirectional fabric-reinforced polybutylene-terephthalate (PBT/GF60) specimens. On the surface of the aluminum specimens, they also manufactured millimeter-sized pins using the Surfi-Sculpt technology and nanometer- and micrometer-sized surface structures with the laser ablation technique. Based on their findings, aluminum-PA/GF15 joints were the weakest regardless of the surface structuring used. They explained this phenomenon with the fact that this composite has fewer glass fibers in it, which makes it less resistant to peeling loads that were generated during the shear tests. The strongest joints were manufactured when aluminum specimens with micrometer-sized surface structures (which were also the fastest to manufacture) were joined with the composite specimens.<sup>[38]</sup> Zhang et al. reached similar shear strength when they used AA7050-type aluminum alloy, the surface of which was modified with the Surfi-Sculpt technique, and short carbon-fiber reinforced PA6 composite specimens. They proved that these protrusions are under shear and bending loads during a shear test, and failure of their joints was mostly caused by the cohesive failure of the protrusions. They also theorized that by optimizing the shape and density of the protrusions, even stronger joints could be manufactured.<sup>[39]</sup>

Lambiase and Genna manufactured joints between AA5053-type aluminum alloy, with a surface structured using a fiber laser, and PEEK specimens using a diode laser. They also measured the temperature evolution in the joining zone with a thermal camera. Based on their observations, joints with a high shear strength can be manufactured above the melting temperature of the PEEK ( $\approx 400$  °C), with a short cycle time to decrease degradation and the formation of bubbles which decrease the strength of the joint and the material itself, too.<sup>[112]</sup> In a later publication, Lambiase and Genna joined AA5053-type aluminum alloy and PVC specimens together using a diode laser and the direct laser joining technique. Based on their preliminary experiments, the two materials they used are chemically incompatible; thus, they manufactured grid-like surface structures on the aluminum specimen using a fiber laser. They again measured the temperature evolution during the joining process and found that regardless of joining speed, when 100 W of laser power was used, the temperature distribution of the aluminum specimen was uniform in the joining zone. However, the PVC could not properly wet the surface of the aluminum, nor could it fill the ditches in the grid-like surface pattern. The strongest joints (15.3 MPa

shear strength on average) were manufactured with a laser power of 200 W and a joining speed of  $100 \text{ mm min}^{-1}$ .<sup>[113]</sup> Schricker et al. manufactured joints between AA6082-type aluminum alloy and PA6.6 specimens. The surface of aluminum was treated with a fiber laser forming grooves along the joining path. In their experiments, they examined the effect of joining speed and measured the temperature in the joining zone using a K-type thermocouple. They also specified the thickness of the melted polymer layer. Based on their tests, increasing joining speed did not change the maximal load-bearing capacity of the joints. However, it changed the failure mode: at slow joining speeds (at  $2 \text{ mm s}^{-1}$ ), the joint was rigid and failed with brittle fracture along the interface, but at higher joining speeds (at and above  $6 \text{ mm s}^{-1}$ ), the joint was tough. The authors explained this phenomenon with lower heat input into and faster cooling of the polymer specimen and changes of the microstructure (the formation of more amorphous regions). Some joined specimens were aged in a furnace, at  $155 \text{ }^\circ\text{C}$  (above the glass transition temperature of the PA6.6) for 1–7 days. The authors stated that the strength of the joints sharply decreased (to about half of that of unaged specimens) even after 1 day of aging. They attributed this to the recrystallization and the consequent embrittlement of the PA material. Aging for more than 1 days did not influence the strength of the joints further.<sup>[114]</sup> Al-Sayyad et al. used Nd:YVO<sub>4</sub> laser welding machine in the pulsed mode to join AA1050-type aluminum (surface treated with a fiber laser) alloy and PA6.6 specimens. They examined the effect of different surface preparation parameters on joint strength: they found a linear correlation between the shear strength and frequency of the laser pulses used during the surface treatment (which also influenced the actual size of the joining surface).<sup>[115]</sup>

During the transmission welding (for reference, see Figure 14) of metal and polymer specimens, it may be necessary to apply so much laser power to properly heat up the metal specimen such that it degrades the polymer material, also making it impossible to form any joints between the specimens. This problem can be averted using highly transparent materials (if possible) or other joining processes. However, Chen et al. recently published a novel technique called ultrasonic-aided laser welding, in which a laser welding machine is combined with an ultrasonic welding machine (Figure 15). With this technique, laser power can be decreased to such an extent that it does not degrade the polymer. At the same time, the ultrasonic welding equipment vibrates the joining zone, which homogenizes the melted polymer and so joints with better strength can be formed.<sup>[136–139]</sup>

### 3.5. In Situ Joining Technologies

#### 3.5.1. Overmolding

IM is one of the most widely used forming technologies in the industry, with which 3D polymer structures can be manufactured in short cycles. During the IM process, polymer granules are melted and then forced into a closed mold under high pressure (Figure 16).<sup>[1,140]</sup>

Advantages of IM are that it is highly automatable; practically no waste is created; it can be used in mass production; and it facilitates the easy recycling of polymer products. Disadvantages include the fact that it is a discontinuous process that requires a lot of investment, as both the tools and the IM machines are expensive.

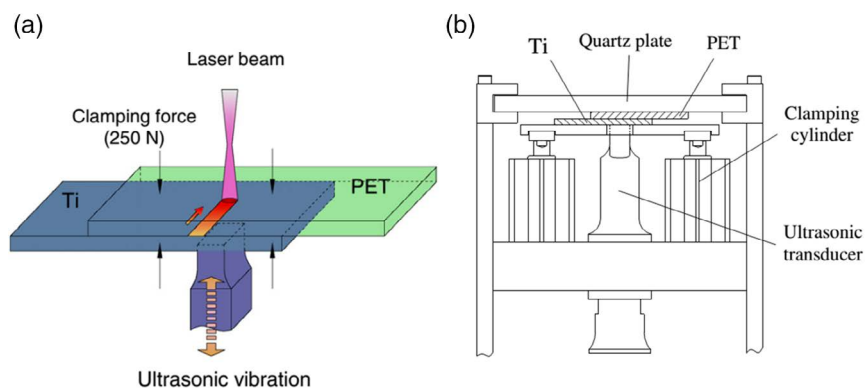


**Figure 15.** Schematic of the a) ultrasonic-aided laser welding joining technology and b) the clamping system used to join metal–polymer specimens. Reproduced with permission.<sup>[136]</sup> 2016, Elsevier Inc.

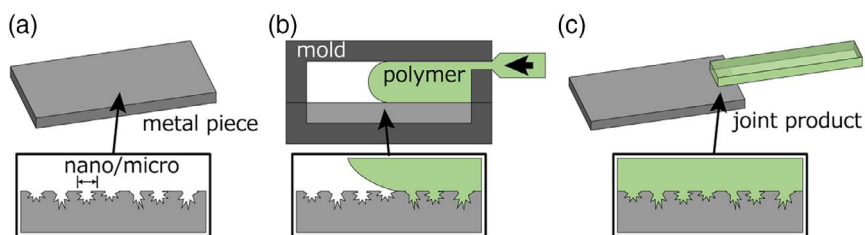


**Figure 16.** Schematic of creating overmolded aluminum–polymer joints: a) metal piece with a prepared surface; b) the polymer melt fills up the surface roughness of the aluminum during the molding process; and c) the final jointed product. Reproduced with permission.<sup>[140]</sup> 2019, Elsevier Inc.

Joints between aluminum and polymer specimens can be created in situ (meaning that the polymer specimen is formed in the same process step that the joint is created) with a modified IM tool and the overmolding technology (Table 7). This process takes advantage of two beneficial properties of IM: melted polymer has a higher wetting ability and thus, the surface roughness ditches of aluminum structures (inserts) placed into the IM tool before the injection cycle can easily be filled up by the polymer melt, forming many shape-connected joints.<sup>[150]</sup>

Luchetta et al. searched for the correlation between the surface structure properties of an AA6082-type aluminum alloy sheet, the process control parameters of an IM cycle, and the joint strength of overmolded aluminum–glass fiber-reinforced PP and PPS (with different fiber contents) specimens. They

prepared the surface of the aluminum specimen with shot peening, during which the surface-hardened and surface structures formed. The strength of the joints was evaluated with shear tests. They found that three main phenomena can happen during a typical overmolding process: first, the polymer melt properly fills up the surface structures of the aluminum specimens (which can be further increased by heating the aluminum specimen), then during the cooling period, the polymer material debonds from the surface of the aluminum because of the difference in thermal expansion coefficients and shrinkage (can be decreased with the use of fiber-reinforced materials), and lastly, short fibers that are stuck in the surface structures of the aluminum decrease shrinkage and increase the effect of shape-connected joints on the global strength of the joint itself.<sup>[141]</sup>

**Table 7.** Materials, surface preparation methods, test parameters, and mechanical properties of joints made by overmolding (n. a. = data not available).

Type and thickness of aluminum component	Type and thickness of polymer component	Surface preparation method	Ultimate failure load or strength of joint ([N] or [MPa])	Test parameters	Ref. no.
AA6082 (3 mm)	PP–GF30–50 (n. a.) PPS–GF40 (n. a.)	Shot peening	0.56–0.72 MPa 0.67–0.97 MPa	Diameter of abrasive material used during shot peening ( $\phi$ 0.1–0.6 mm) Preheating of aluminum (250–400 °C) Injection speed (just for PPS–GF, 80–120 mm s <sup>-1</sup> )	[141]
AA1100 (0.5 and 1.5 mm)	PS (4.5 mm)	Grinding with emery paper + addition of elastomer-based primer material (by Metsan Inc.)	27–35 MPa	Amount of SEBS–g–MA additive (5 and 15%)	[142]
AA5052 (1.5 mm)	PBT–GF30 (3 mm)	Chemical treatment (by Nano Molding Technology, Taiseiplas)	600–900 N	Overlap distance (5 and 10 mm) Injection pressure (60–120 MPa) Holding pressure (20–60 MPa) Injection speed (150–600 mm min <sup>-1</sup> )	[143]
AA6061 (2 mm)	PP (2 mm)	Sandblasting	0–250 N	Preheating of aluminum (60–150 °C)	[144]
AA6061 (2 mm)	PPS–GF30 (2 mm)	Sandblasting + cleaning the surface in an ultrasonic bath in ethanol	60–660 N	Typical size of abrasive materials used for sandblasting (0.3–2 mm) Preheating of aluminum (30–150 °C)	[145]
AA6061 (2 mm)	PPS–GF30 (2 mm)	Anodization Coating with a silane-based compound	1–7.7 MPa	Amperage of anodization (0.8–1.4 A dm <sup>-2</sup> ) Anodization time (15–75 min) Curing time of the silane compound (0–60 min) Curing temperature of the silane compound (100–200 °C)	[146]
AA5754 (1 mm)	PA6–GF30 (2 mm)	Electrochemical treatment of aluminum in nitric and then hydrochloric acid	4–22 MPa	Type of acid (Nitric or hydrochloric acid) Amperage used during the treatment (1.56 and 2.06 mA mm <sup>-2</sup> )	[147]
AA5052 (1.5 mm)	PBT (3 mm)	Shot peening	2–15 MPa	Type and typical size of abrasive materials used for shot peening (glass and aluminum pieces, 47.5–256 $\mu$ m), peening pressure (0.3–1 MPa) Nozzle temperature (240–280 °C) Injection speed (10–300 mm s <sup>-1</sup> ) Holding pressure (1–90 MPa)	[148]
AA5005 (1.5 mm)	TPE–S (1.5 mm)	Cleaning the surface with ethanol	3.3–5.5 MPa	Temperature and length of heat treatment (80–150 °C, 2–16 h)	[149]
AA5052 (1.5 mm)	PBT–GF30 (3 mm)	Anodizing	3–22 MPa	Anodization time (30 and 60 min) Injection speed (10–300 mm s <sup>-1</sup> ) Injection pressure (20–110 MPa)	[140]

Altan and Yavuz manufactured joints between AA1100-type aluminum alloy (with two thicknesses) and polystyrene (PS) and maleic–anhydride-grafted styrene ethylene butylene styrene (SEBS-g-MA) specimens by overmolding. They evaluated the effect of injection pressure on the deformation of the aluminum specimens and the bending strength of the aluminum–polymer joints. They found that the aluminum–SEBS-g-MA joints had greater bending strength and when over 60 MPa of injection pressure, the 0.5 mm-thick aluminum specimens failed in the mold.<sup>[142]</sup> Kimura et al. manufactured joints between AA5052-type aluminum alloy and short glass fiber-reinforced PBT using overmolding. They used the so-called Nano Molding Technology of Taiseiplas to prepare the surface of the aluminum specimens before joining, which produced nanoscale surface structures. They found that the shear strength of the aluminum–polymer joints was influenced positively when packing pressure was increased and negatively when injection speed was decreased.<sup>[143]</sup> Li et al. modified a mold and its tempering system so that the temperature of the aluminum specimen placed inside the mold could be changed rather quickly (Figure 17). Using this technique, they managed to form stronger joints between aluminum and polymer, because the temperature gradient between the aluminum and the melted polymer was less harsh and the melted polymer did not immediately freeze and was able to fill up the surface structures of the aluminum specimen better.<sup>[144,145]</sup> In their first article, Li et al. manufactured joints between AA6061-type aluminum alloy (prepared with sandblasting) and PP specimens using overmolding. They found that no joint could be made, when the temperature of the aluminum was set to or below 60 °C, and that the strongest joints were manufactured at 120 °C.<sup>[144]</sup> In their second article, Li et al. manufactured joints between AA6061-type aluminum alloy (prepared by shot peening with different-sized abrasive materials) and short glass fiber-reinforced PPS composite specimens. They found that increasing the temperature of the aluminum specimen beneficially influenced the strength of the joint in this case too. Furthermore, they specified the ideal surface roughness and surface structure density with respect to joint strength.<sup>[145]</sup>

In a later article, Li et al. manufactured joints between AA6061-type aluminum alloy (prepared with anodizing) and short glass fiber-reinforced PPS composite specimens by

overmolding. After anodizing, they dipped the aluminum specimen into a solution containing a silane-based adhesion-promoting compound. They then evaluated the effect of anodizing (current value and anodizing time) and curing process parameters (curing time and temperature for the silane-based compound) on the strength of the aluminum–polymer joints.<sup>[146]</sup> Kleffel and Drummer manufactured so-called T-joints between AA5754-type aluminum alloy (prepared with an electrochemical method) and short glass fiber-reinforced PA6 specimens. They used a built-in induction-based tempering system to heat the aluminum specimen during the IM phase of the overmolding process. Because of their nature and geometric structure, the tensile strength of the joints could be measured. Kleffel and Drummer used an optical microscope and a scanning electron microscope to measure the effective joining area (undercuts and surface roughness) on the surfaces of tested specimens.<sup>[147]</sup> Kajihara et al. manufactured overlapped joints using AA5052-type aluminum alloy (prepared with shot peening) and PBT specimens. They used glass and aluminum grains and pellets of different sizes, and also different air pressures during the surface preparation phase, and thus they created surface structures with characteristic values reaching into the nanometer range. They found that increasing the air pressure and the temperature of the melted polymer positively influenced joint strength, whereas average surface roughness and injection speed also had an effect on strength.<sup>[148]</sup> Frick et al. used AA5005-type aluminum alloy (with a degreased surface) and styrene-based thermoplastic polymer (TPE) specimens to manufacture double lap joints. They found that the strength and the water permeability of the joints could be increased by heat treating the joints at 120 °C for 2 h. This also changed the failure mode of the joints from debonding on the joining surface to cohesive failure of the TPE specimens.<sup>[149]</sup> Kadoya et al. manufactured overlapped joints between AA5052-type aluminum alloy (prepared with anodizing) and short glass fiber-reinforced PBT specimens. Based on the tests they conducted, they found that increasing injection speed and also decreasing injection pressure at high injection speeds decreased the strength of the joints. They explained this phenomenon with the degradation of the melted polymer due to increased shear and melt temperatures at high injection speeds.<sup>[140]</sup>

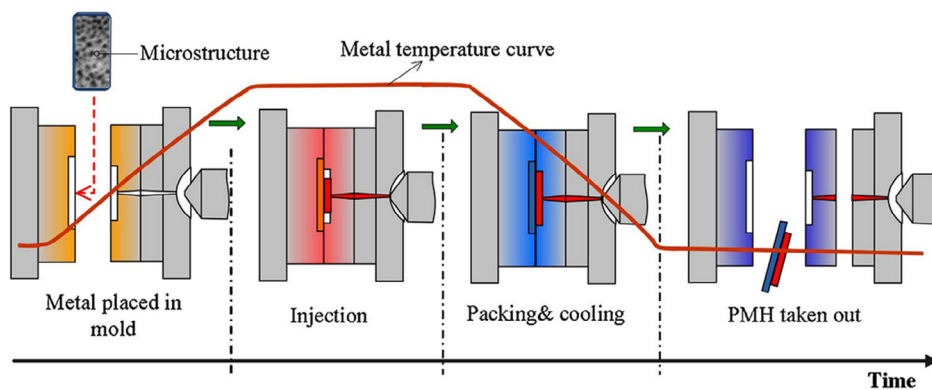


**Figure 17.** The so-called Micro-IJT molding technology, during which the temperature of the aluminum specimen can be changed rapidly. Reproduced with permission.<sup>[142]</sup> 2017, Elsevier Inc.

### 3.5.2. 3D Printing

Fused deposition modeling (FDM) is based on melting and then depositing a polymer filament (a virtually endless, fiber-like material) layer by layer onto a heated bed. The melting is done by a small extruder head equipped with a nozzle, into which the filament is pushed during the FDM printing process. The melted material is then deposited onto a heated bed or onto a previous layer of already solidified material by an extruder head working in the X–Y axis (the bed can also move vertically, thus providing the possibility of manufacturing 3D structures). It is essential that the newly deposited material is properly bonded to the previous layer and that a filament with an appropriate diameter is used, so that enough material is supplied for the building process. This can be influenced by the temperature of the printing process and the pressure, with which the melted polymer is pushed through the extruder head. It may be necessary (based on model geometry) to use supports which can be printed from the material that the model is made of (but with a looser structure), or another material can also be used. However, in this case, an FDM machine with two or more extruder heads must be used (Figure 18). It is possible to manufacture aluminum–polymer joints using the FDM technology by building the polymer structure on the aluminum specimen instead of the building table of the FDM printer (Figure 18b).<sup>[151]</sup>

Advantages of the FDM technology include good value for price, the possibility of manufacturing complex 3D structures using one or more material source (if a dual-head FDM printer is available). Disadvantages include poor accuracy (minimum

layer height is 100  $\mu\text{m}$ , even on the most precise machines) and slow building times, depending on the complexity of the model and the chosen layer height.<sup>[151]</sup>

Falck et al. presented a modified 3D printing (FDM) technology (the so-called AddJoining technique), with which aluminum–polymer joints can be in situ manufactured (Table 8). They prepared AA2024-type aluminum alloy specimens by degreasing and then coating their surface with a solution containing the polymer material (ABS and PA6) that they later used in the AddJoining process (Figure 18). They proved that endless rovings of carbon fibers, coated with thermoplastic polymer, could also be used to manufacture aluminum–polymer joints. The average shear strength of the overlapped joints where the authors used PA6-coated aluminum sheets and PA6-coated carbon rovings was 21.9 MPa, which is about twice as strong as adhesively bonded or induction-welded joints used in the industry. Using fracture analysis, they proved that the failure of the joints caused delamination between the PA6 coating on the surface of the aluminum and PA6/CF layers where they found micro-sized cavities. They theorized that with further thermal or thermomechanical treatment, the size of these cavities and voids could be decreased, and thus, joint strength could be further increased.<sup>[151]</sup> In a later article, Falck et al. manufactured overlapped joints between AA2024-type aluminum alloy (prepared with sandblasting and then coated with ABS in different layer thicknesses) and ABS material using the AddJoining technique. They compared the strength of these joints with the tensile strength of 3D-printed ABS specimens and used optical and SEM to study the microstructure of the aluminum–ABS joints. They found that the

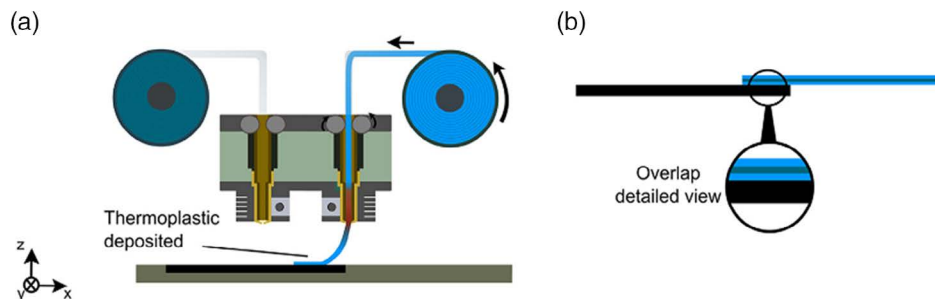


**Figure 18.** Manufacturing aluminum–polymer joints using 3D printing: a) laying individual layers and b) the finished hybrid structure. Reproduced with permission.<sup>[148]</sup> 2018, Elsevier Inc.

**Table 8.** Materials, surface preparation methods, test parameters, and mechanical properties of joints made by 3D printing.

Type and thickness of aluminum-joining partner	Type and thickness of polymer-joining partner	Surface preparation method	Ultimate failure load or strength of joint ([N] or [MPa])	Test parameters	Ref. no.
AA2024 (2 mm)	ABS ( $\varnothing$ 1.75 mm)	Sandblasting	5–5.6 MPa	Materials used for 3D printing	[151]
	PA6 + CF ( $\varnothing$ 0.38 mm)	Coating with ABS and PA6	20.8–23 MPa		
AA2024 (2 mm)	ABS ( $\varnothing$ 1.75 mm)	Sandblasting Coating with ABS	910–1686 N	ABS content of coating material (5–25 wt%) Nozzle temperature (230–280 °C) Layer thickness (0.1–0.3 mm) Printing speed (20–60 mm s <sup>-1</sup> ) Number of layers (2–22 layers)	[152]

failure of the compared specimens occurred at about the same level of stress and that the strength of the 3D-printed joints was mainly influenced by the speed of the printing process. They explained the latter with the fact that when layers are added quickly, there is less time for the material to cool down; thus, better consolidation and greater diffusion between layers can be achieved.<sup>[152]</sup>

#### 4. Conclusion and Outlook

With the spread of Industry 4.0 and as materials science and technology developed, more automated manufacturing processes were used in the industry. As aluminum and polymers as low-density engineering materials are used more widely, there is a growing need for technologies to join them. These aluminum–polymer hybrid structures are expected to be widely used in numerous industries, especially in the aerospace industry, where weight reduction is of paramount importance for economical operation.<sup>[2,153–155]</sup> A thorough literature review reveals that there are numerous joining technologies that can be used to create aluminum–polymer joints.

In the past years new joining technologies (such as friction spot joining) have been developed and existing joining technologies have been modified with the aim of producing joints between metals and polymers in short cycles and with good reproducibility, with the use of simple parts and equipment. The reliability of these technologies is not entirely proved yet, and as a result, they have not yet become widespread in industrial use. The use of aluminum–polymer joints manufactured with technologies that are ready for mass production (laser welding, ultrasonic welding) is not widespread either according to the literature. In this article, in addition to presenting the state of the art of highly productive joining technologies for aluminum and polymer materials, we introduced a new categorization approach for joining technologies that is based on micro- and/or macro-structural changes in the polymer specimen during joining.

Another important part of joining aluminum and polymer specimens (in addition to the mechanical properties of joints) is surface preparation, as without the proper preparation of the aluminum before joining, the strength of aluminum–polymer bonds is too weak in most cases. There is a large number of technologies available for the surface preparation of aluminum. These can be physical or chemical in action principle. According to the novel grouping method also presented in this Review Article, the surface preparation techniques (which influence surface roughness and thus the amount of shape-connected joints) can also be categorized into subtractive, additive, or surface-modifying subcategories.

There are a lot of variables which are known to have an influence on the strength of hybrid aluminum–polymer joints, but their action principle and the magnitude of their influence still require further study. Some of these variables are material parameters, whereas others are technological parameters. In addition to fine tuning and improving the joining technologies and the joining processes themselves, a lot of research on the materials is still needed, as the literature to date lacks a systematic approach to the topic.

Some of the most important hot topics in hybrid metal–polymer joints are the effects of microstructural and macrostructural changes in the aluminum and the polymer during joining. However, for example, the effect of shrinkage of the polymer and the effect of possible changes in the surface oxide layer and the crystalline structure of the aluminum caused by heat have not been fully researched yet. In the vehicle industry, which will use aluminum–polymer joints in high quantities, joints must be solid, watertight, and corrosion resistant. These properties of hybrid joints have not yet been investigated deeply enough. Furthermore, neither the long-term behavior of hybrid structures under normal loads (creep, high-frequency loads, impact loads etc.), nor the applicability of thick (more than 5 mm) thermoplastic and fiber-reinforced composite materials have been extensively investigated. These problems prevent the regular industrial use of even the fastest and most easily automatable joining technologies (laser and ultrasonic welding) and hybrid aluminum–polymer joints. However, based on the increasing attention (as presented in this Review Article), the joining of dissimilar materials in one step, using a single welding machine, and the investigation of these joints will surely remain a hot topic in the coming years.

#### Acknowledgements

This work was supported by the National Research, Development and Innovation Fund under grant no. TUDFO/51757/2019-ITM, Thematic Excellence Program.

#### Conflict of Interest

The authors declare no conflict of interest.

#### Keywords

aluminum, joining technologies, surface preparation, thermoplastic polymers, welding

Received: December 30, 2019

Revised: April 7, 2020

Published online: May 28, 2020

- [1] S. T. Amancio-Filho, L. Blaga, *Joining of Polymer-Metal Hybrid Structures – Principles and Applications*, John Wiley & Sons, Inc., Hoboken, NJ **2018**.
- [2] D. Lehmhus, A. von Hehl, J. Hausmann, K. Kayvantash, R. Alderliesten, J. Hohe, *Adv. Eng. Mater.* **2019**, 1900056, 1.
- [3] BMW Electric Vehicles–BMW i3 Employs New Joining Technology for CFRP Parts, <https://www.plastics.gl/automotive/bmw-i3-employs-new-joining-technology-for-cfrp-parts/> (accessed: May 2020).
- [4] A. Pramanik, A. K. Basak, Y. Dong, P. K. Sarker, M. S. Uddin, G. Littlefair, A. R. Dixit, S. Chattopadhyaya, *Composites, Part A* **2017**, 101, 1.
- [5] PMJoin–Development of a Direct Laser Joining of Hybrid Plastic-Metal Components for Industrial Applications, **2016**.
- [6] R. Patwa, H. J. Herfurth, S. Heinemann, G. Newaz, presented at Micromanufacturing Conf. & Exhibits, Minneapolis, MN, April **2009**.
- [7] K. Scholten, E. Meng, *Lab Chip* **2015**, 15, 4256.

- [8] S. Ebnesajjad, *Handbook of Adhesives and Surface Preparation*, Elsevier, Oxford **2011**.
- [9] A. Baldan, *J. Mater. Sci.* **2004**, 39, 1.
- [10] A. Pizzi, K. L. Mittal, *Handbook of Adhesive Technology*, Marcel Dekker, Inc., New York **2003**.
- [11] *ASM Engineered Materials Handbook, Vol 3: Adhesives and Sealants* (Ed: C. A. Dostal), ASM International, CRC Press, Ohio, USA **1990**.
- [12] G. W. Critchlow, D. M. Brewis, *Int. J. Adhes. Adhes.* **1996**, 16, 255.
- [13] M. Stafe, A. Marcu, N. N. Puscas, *Pulsed Laser Ablation of Solids – Basics, Theory and Applications*, Springer Verlag, Berlin-Heidelberg **2014**.
- [14] A. Rudawska, I. Danczak, M. Müller, P. Valasek, *Int. J. Adhes. Adhes.* **2016**, 70, 176.
- [15] P. Molitor, V. Barron, T. Young, *Int. J. Adhes. Adhes.* **2001**, 21, 129.
- [16] J. Byskov-Nielsen, P. Balling, *Appl. Surf. Sci.* **2009**, 255, 5591.
- [17] A. T. T. Nguyen, M. Brandt, A. C. Orifici, S. Feih, *Int. J. Adhes. Adhes.* **2016**, 66, 81.
- [18] J. J. Narbon, C. Moreno-Díaz, J. M. Arenas, *Colloids Surf., A* **2019**, 560, 323.
- [19] N. Anagreh, A. Al Robaidi, *Jordan J. Mech. Ind. Eng.* **2010**, 4, 330.
- [20] Y. Wu, J. Lin, B. E. Carlson, P. Lu, M. P. Balogh, N. P. Irish, Y. Mei, *Surf. Coat. Technol.* **2016**, 304, 340.
- [21] G. V. Kuznetsov, D. V. Feoktistov, E. G. Orlova, K. Batishcheva, S. S. Ilenok, *Appl. Surf. Sci.* **2019**, 469, 974.
- [22] C.-V. Ngo, D.-M. Chun, *Appl. Surf. Sci.* **2018**, 435, 974.
- [23] J. Karger-Kocsis, L. Lendvai, *J. Appl. Polym. Sci.* **2018**, 135, 1.
- [24] M. G. Z. Khorasani, D. Silbernagl, P. Szymoniak, V.-D. Hodoroaba, H. Sturm, *Polymer* **2019**, 164, 174.
- [25] D. M. Heaney, *Handbook of Metal Injection Molding*, Woodhead Publishing Ltd., Cambridge **2012**.
- [26] B. Mezrag, F. D. Beaume, S. Rouquette, M. Benachour, *Sci. Technol. Weld. Joining* **2018**, 23, 508.
- [27] S. Ucsnik, M. Scheerer, S. Zaremba, D. H. Pahr, *Composites, Part A* **2010**, 41, 369.
- [28] S. Stelzer, S. Ucsnik, G. Pinter, *Int. J. Fatigue* **2015**, 81, 37.
- [29] S. Stelzer, S. Ucsnik, G. Pinter, *Composites, Part A* **2016**, 88, 39.
- [30] P. N. Parkes, R. Butler, J. Meyer, A. de Oliveira, *Compos. Struct.* **2014**, 118, 250.
- [31] R. F. Wegman, J. V. Twisk, *Surface Preparation Techniques for Adhesive Bonding*, William Andrew Inc., Oxford **2013**.
- [32] A. Mian, G. Newaz, T. Mahmood, G. Auner, *J. Mater. Sci.* **2007**, 42, 8150.
- [33] T. Sultana, G. Newaz, G. L. Georgiev, R. J. Baird, G. W. Auner, R. Patwa, H. J. Herfurth, *Thin Solid Films* **2010**, 518, 2632.
- [34] J. Blackburn, P. Hilton, *Phys. Procedia* **2011**, 12, 529.
- [35] P. Hilton, L. Nguyen, *J. Laser Appl.* **2008**, 61.
- [36] A. L. Buxton, B. G. I. Dance, presented at ISEC Congress of ASM International, St. Paul, MN, August **2005**.
- [37] A. N. Fuchs, F. X. Wirth, P. Rinck, M. F. Zaeh, *Phys. Procedia* **2014**, 56, 801.
- [38] A. Heckert, M. F. Zaeh, *Phys. Procedia* **2014**, 56, 1171.
- [39] Z. Zhang, J. Shan, X. Tan, J. Zhang, *Int. J. Adv. Manuf. Technol.* **2016**, 90, 3465.
- [40] L. Bónová, A. Zahoranová, D. Kováčik, M. Zahoran, M. Mičušík, M. Černák, *Appl. Surf. Sci.* **2015**, 331, 79.
- [41] L. Muñoz, F. Pineda, C. Martínez, M. Sancy, M. Urzua, M. Flores, M. V. Encinas, M. A. Páez, *Surf. Coat. Technol.* **2019**, 358, 435.
- [42] J. V. Esteves, S. M. Goushegir, J. F. dos Santos, L. B. Canto, E. Hage, S. T. Amancio-Filho, *Mater. Des.* **2015**, 66, 437.
- [43] S. M. Goushegir, J. F. dos Santos, S. T. Amancio-Filho, *Mater. Des.* **2014**, 54, 196.
- [44] S. M. Goushegir, J. F. dos Santos, S. T. Amancio-Filho, *Mater. Des.* **2015**, 83, 431.
- [45] N. M. André, S. M. Goushegir, J. F. dos Santos, L. B. Canto, S. T. Amancio-Filho, *Composites, Part B*, **2016**, 94, 197.
- [46] F. Lambiase, A. Paoletti, V. Grossi, A. D. Ilio, *J. Manuf. Process.* **2017**, 29, 221.
- [47] F. Lambiase, A. Paoletti, *Compos. Struct.* **2018**, 189, 70.
- [48] Y. Ogawa, H. Akebono, K. Tanaka, A. Sugeta, *Sci. Technol. Weld. Joining* **2018**, 24, 235.
- [49] N. M. Andre, J. F. dos Santos, S. T. Amancio-Filho, *Materials*, **2019**, 12, 891.
- [50] P. K. Rana, R. G. Narayanan, S. V. Kailas, *J. Mater. Process. Technol.* **2018**, 252, 511.
- [51] P. K. Rana, R. G. Narayanan, S. V. Kailas, in *Strengthening and Joining by Plastic Deformation* (Eds.: U. S. Dixit, R. G. Narayanan), Springer Nature, Singapore, **2019**.
- [52] P. K. Rana, R. G. Narayanan, S. V. Kailas, *Thin-Walled Struct.* **2019**, 138, 415.
- [53] S. Aliasghari, M. Ghorbani, P. Skeldon, H. Karami, M. Movahedi, *Surf. Coat. Technol.* **2017**, 313, 274.
- [54] S. Aliasghari, P. Skeldon, X. Zhou, M. Ghorbani, *Int. J. Adhes. Adhes.* **2019**, 92, 65.
- [55] S. Aliasghari, P. Skeldon, X. Zhou, T. Hashimoto, *Mater. Sci. Eng., B* **2019**, 245, 107.
- [56] X. Xiong, M. Li, S. Ji, D. Yan, Z. Liu, *Adv. Eng. Mater.* **2019**, 21, 1900510.
- [57] I. T. Abdullah, S. K. Hussein, *Int. J. Struct. Integr.* **2019**, 10, 469.
- [58] H. K. Pabandi, M. Movahedi, A. H. Kokabi, *Compos. Struct.* **2017**, 174, 59.
- [59] Y. Huang, X. Meng, Y. Xie, J. Li, L. Wan, *Composites, Part B*, **2019**, 163, 217.
- [60] N. Z. Borba, L. Blaga, J. F. dos Santos, S. T. Amancio-Filho, *Mater. Lett.* **2018**, 215, 31.
- [61] L. Blaga, J. F. dos Santos, R. Bancila, S. T. Amancio-Filho, *Constr. Build. Mater.* **2015**, 80, 167.
- [62] C. F. Rodrigues, L. A. Blaga, J. F. dos Santos, L. B. Canto, E. Hage, S. T. Amancio-Filho, *J. Mater. Process. Technol.* **2014**, 214, 2029.
- [63] J. Min, Y. Li, J. Li, B. E. Carlson, J. Lin, *Int. J. Adv. Manuf. Technol.* **2014**, 76, 1403.
- [64] F. C. Liu, J. Liao, K. Nakata, *Mater. Des.* **2014**, 54, 236.
- [65] K. Nagatsuka, S. Yoshida, A. Tsuchiya, K. Nakata, *Composites, Part B*, **2015**, 73, 82.
- [66] H. S. Bang, A. Das, S. Lee, H. S. Bang, *IOP Conf. Ser.: Mater. Sci. Eng.* **2018**, 369, 012033.
- [67] A. Das, H. S. Bang, H. S. Bang, *IOP Conf. Ser.: Mater. Sci. Eng.* **2018**, 369, 012032.
- [68] F. C. Liu, P. Dong, in *Friction Stir Welding and Processing X* (Ed.: Y. Hovansky), Springer International Publishing AG, Cham **2019**.
- [69] F. C. Liu, P. Dong, W. Lu, K. Sun, *Appl. Surf. Sci.* **2019**, 466, 202.
- [70] F. Khodabakhshi, M. Haghshenas, S. Sahraeinejad, J. Chen, B. Shalchi, J. Li, A. P. Gerlich, *Mater. Charact.* **2014**, 98, 73.
- [71] F. Khodabakhshi, M. Haghshenas, J. Chen, B. S. Amirkhiz, J. Li, A. P. Gerlich, *Sci. Technol. Weld. Joining* **2016**, 22, 182.
- [72] R. Moshwan, S. M. Rahmat, F. Yusof, M. A. Hassan, M. Hamdi, M. Fadzil, *Int. J. Mater. Res.* **2015**, 105, 1.
- [73] H. Shahmiri, M. Movahedi, A. H. Kokabi, *Sci. Technol. Weld. Joining* **2016**, 22, 120.
- [74] A. R. Patel, D. J. Kotadiya, J. M. Kapopara, C. G. Dalwadi, N. P. Patel, H. G. Rana, *Mater. Today: Proc.* **2018**, 5, 4242.
- [75] W. Ratanathavorn, A. Melander, *Sci. Technol. Weld. Joining* **2015**, 20, 222.
- [76] H. A. Derazkola, R. K. Fard, F. Khodabakhshi, *Weld. World* **2018**, 62, 117.
- [77] H. A. Derazkola, F. Khodabakhshi, A. Simchi, *Sci. Technol. Weld. Joining* **2017**, 23, 35.
- [78] H. A. Derazkola, A. Simchi, *Thin-Walled Structures* **2019**, 135, 376.
- [79] H. A. Derazkola, M. Elyasi, *J. Manuf. Process.* **2018**, 35, 88.

- [80] Y. Huang, X. Meng, Y. Wang, Y. Xie, L. Zhou, *J. Mater. Process. Technol.* **2018**, 257, 148.
- [81] Y. Huang, X. Meng, Y. Xie, J. Li, L. Wan, *Composites, Part A* **2018**, 112, 328.
- [82] Y. Huang, X. Meng, Y. Xie, J. Li, X. Si, Q. Fan, *J. Mater. Process. Technol.* **2019**, 268, 80.
- [83] S. K. Sahu, M. Panda, R. P. Mahto, S. K. Pal, K. Pal, P. Dash, in *Proc. of the 10th Int. Conf. on Precision, Meso, Micro and Nano Engineering*, Vol. 1, Indian Institute of Technology, Madras, Chennai, India **2018**.
- [84] M. J. Troughton, *Handbook of Plastics Joining A Practical Guide*, 2nd edn., William Andrew Inc., Norwich, NY **2008**.
- [85] D. Lohwasser, Z. Chen, *Friction Stir Welding – From Basics to Application*, Woodhead Publishing Ltd., Cambridge **2010**.
- [86] M. P. Mubiayi, E. T. Akinlabi, M. E. Makhatha, *Current Trends in Friction Stir Welding (FSW) and Friction Stir Spot Welding (FSSW) – An Overview and Case Studies*. Springer International Publishing AG, Cham **2019**.
- [87] Y. Huang, X. Meng, Y. Xie, L. Wan, Z. Lv, J. Cao, J. Feng, *Composites, Part A* **2018**, 105, 235.
- [88] R. Kumar, R. Singh, I. P. S. Ahuja, R. Penna, L. Feo, *Composites, Part B*, **2018**, 137, 1.
- [89] Z. Kiss, T. Czigány, *Period. Polytech., Mech. Eng.* **2007**, 51, 15.
- [90] J. Rotheiser, *Joining of Plastics – Handbook for Designers and Engineers*, Carl Hanser Verlag, Munich **1999**.
- [91] P. Mitschang, R. Velthuis, S. Emrich, M. Kopnarski, *J. Thermoplast. Compos. Mater.* **2009**, 22, 767.
- [92] P. Mitschang, R. Velthuis, M. Didi, *Adv. Eng. Mater.* **2013**, 15, 804.
- [93] M. Didi, S. Emrich, P. Mitschang, M. Kopnarski, *Adv. Eng. Mater.* **2013**, 15, 821.
- [94] K. Szallies, M. Bielenin, K. Schricker, J. P. Bergmann, C. Neudel, *Weld. World* **2019**, 63, 1145.
- [95] A. Roesner, S. Scheik, A. Olowinsky, A. Gillner, U. Reisgen, M. Schleser, *Phys. Procedia* **2011**, 12, 370.
- [96] P. Mitschang, R. Rudolf, M. Neitzel, *J. Thermoplast. Compos. Mater.* **2002**, 15, 127.
- [97] T. Bayerl, M. Duhovic, P. Mitschang, D. Bhattacharyya, *Composites, Part A* **2014**, 57, 27.
- [98] F. Balle, G. Wagner, D. Eifler, *Materialwiss. Werkstofftech.* **2007**, 38, 934.
- [99] F. Balle, G. Wagner, D. Eifler, *Adv. Eng. Mater.* **2009**, 11, 35.
- [100] G. Wagner, F. Balle, D. Eifler, *Adv. Eng. Mater.* **2013**, 15, 792.
- [101] R.-Y. Yeh, R.-Q. Hsu, *Int. J. Adhes. Adhes.* **2016**, 65, 28.
- [102] A. Al-Obaidi, C. Majewski, in *Transactions on Intelligent Welding Manufacturing* (Ed.: S. Chen), Springer Nature, Singapore **2019**.
- [103] U. F. Dal Conte, I. F. Villegas, J. Tachon, *J. Compos. Mater.* **2019**, 53, 2607.
- [104] F. Staab, F. Balle, *Ultrasonics* **2018**, 93, 139.
- [105] K.-W. Jung, Y. Kawahito, M. Takahashi, S. Katayama, *J. Laser Appl.* **2013**, 13, 032003.
- [106] H. L. Gower, R. R. G. M. Pieters, I. M. Richardson, *J. Laser Appl.* **2006**, 18, 35.
- [107] Y. Farazila, Y. Miyashita, W. Hua, Y. Mutoh, Y. Otsuka, *J. Laser Micro/Nanoeng.* **2011**, 6, 69.
- [108] P. Amend, S. Pfindel, M. Schmidt, *Phys. Procedia* **2013**, 41, 98.
- [109] F. Yusof, M. Yukio, M. Yoshiharu, M. H. Abdul, *Mater. Des.* **2012**, 37, 410.
- [110] Z. Zhang, J.-G. Shan, X.-H. Tan, J. Zhang, *Int. J. Adhes. Adhes.* **2016**, 70, 142.
- [111] C. Lamberti, T. Solchenbach, P. Plapper, W. Possart, *Phys. Procedia* **2014**, 56, 845.
- [112] F. Lambiase, S. Genna, *Int. J. Adhes. Adhes.* **2018**, 84, 265.
- [113] F. Lambiase, S. Genna, *Opt. Laser Technol.* **2018**, 107, 80.
- [114] K. Schricker, M. Stambke, J. P. Bergmann, K. Bräutigam, *Int. J. Polym. Sci.* **2016**, 2016, 5301081.
- [115] A. Al-Sayyad, J. Bardou, P. Hirschmann, K. Santos, L. Houssiau, P. Plapper, *Proc. CIRP*, **2018**, 74, 495.
- [116] R. Patwa, Y. Lu, H. Herfurth, S. Heinemann, K. Washio, W. Hoving, S. Ehrenmann, G. Newaz, J. Amako, R. J. Baird, W. Pfleging, *Proc. SPIE 7202*, **2009**.
- [117] A. Fortunato, G. Cuccolini, A. Ascari, L. Orazi, G. Campana, G. Tani, *Int. J. Mater. Form.* **2010**, 3, 1131.
- [118] A. Bauernhuber, T. Markovits, *Phys. Procedia* **2012**, 39, 108.
- [119] K.-W. Jung, Y. Kawahito, M. Takahashi, S. Katayama, *Mater. Des.* **2013**, 47, 179.
- [120] C.-W. Chan, G. C. Smith, *Mater. Des.* **2016**, 103, 278.
- [121] J. Jiao, Q. Wang, F. Wang, S. Zan, W. Zhan, *J. Mater. Process. Technol.* **2017**, 240, 362.
- [122] J. Rauschenberger, A. Cenigaonandia, J. Keseberg, F. Dorsch, D. Vogler, U. Gubler, F. Liébana, *Proc. SPIE 9356* **2015**.
- [123] S. Katayama, Y. Kawahito, *Scr. Mater.* **2008**, 59, 1247.
- [124] Y. Miyashita, M. Takahashi, M. Takemi, K. Oyama, Y. Mutoh, H. Tanaka, *J. Solid Mech. Mater. Eng.* **2009**, 3, 409.
- [125] W. Tillmann, A. Elrefaey, L. Wojarski, *Materialwiss. Werkstofftech.* **2010**, 41, 879.
- [126] F. Yusof, Y. Mutoh, Y. Miyashita, *Adv. Mater. Res.* **2010**, 129–131, 714.
- [127] X. Wang, X. Song, M. Jiang, P. Li, Y. Hu, K. Wang, H. Liu, *Opt. Laser Technol.* **2012**, 44, 656.
- [128] T. Sano, S. Iwasaki, Y. Ozeki, K. Itoh, A. Hirose, *Mater. Trans.* **2013**, 54, 926.
- [129] C. Engelmann, J. Eckstaedt, A. Olowinsky, M. Aden, V. Mamuschkin, *Phys. Procedia* **2016**, 83, 1118.
- [130] R. Borrisutthekul, A. Saengsai, P. Mitsomwang, *Key Eng. Mater.* **2016**, 719, 142.
- [131] F. Lambiase, S. Genna, *Opt. Laser Technol.* **2017**, 88, 205.
- [132] D. G. Georgiev, R. J. Baird, G. Newaz, G. Auner, R. Witte, H. Herfurth, *Appl. Surf. Sci.* **2004**, 236, 71.
- [133] J. P. Bergmann, M. Stambke, *Phys. Procedia* **2012**, 39, 84.
- [134] E. Rodríguez-Vidal, C. Sanz, C. Soriano, J. Leunda, G. Verhaeghe, *J. Mater. Process. Technol.* **2016**, 229, 668.
- [135] E. Rodríguez-Vidal, C. Sanz, J. Lambarri, J. Renard, V. Gantchenko, *Phys. Procedia* **2016**, 83, 1110.
- [136] Y. J. Chen, T. M. Yue, Z. N. Guo, *Mater. Des.* **2016**, 110, 775.
- [137] Y. J. Chen, T. M. Yue, Z. N. Guo, *J. Mater. Process. Technol.* **2017**, 249, 441.
- [138] Y. J. Chen, T. M. Yue, Z. N. Guo, *J. Manuf. Process.* **2018**, 31, 356.
- [139] Y. J. Chen, T. M. Yue, Z. N. Guo, US patent no 2017/0320167A1, **2017**.
- [140] S. Kadoya, F. Kimura, Y. Kajihara, *Polym. Test.* **2019**, 75, 127.
- [141] G. Lucchetta, F. Marinello, P. F. Bariani, *CIRP Ann.* **2011**, 60, 559.
- [142] M. Altan, B. Yavuz, *Acta Phys. Pol., A* **2016**, 129, 639.
- [143] F. Kimura, S. Kadoya, Y. Kajihara, *Precis. Eng.* **2016**, 45, 203.
- [144] X. Li, F. Liu, N. Gong, P. Huang, C. Yang, *J. Mater. Process. Technol.* **2017**, 249, 386.
- [145] X. Li, F. Liu, N. Gong, C. Yang, B. Wang, *Compos. Struct.* **2018**, 184, 545.
- [146] X. Li, D. Xu, N. Gong, Z. Xu, L. Wang, W. Dong, *Mater. Des.* **2019**, 179, 107875.
- [147] T. Kleffel, D. Drummer, *Composites, Part B*, **2017**, 117, 20.
- [148] Y. Kajihara, Y. Tamura, F. Kimura, G. Suzuki, N. Nakura, E. Yamaguchi, *CIRP Ann.* **2018**, 67, 591.
- [149] A. Frick, S. Aldinger, M. Spadaro, in *Euro Hybrid Materials and Structures 2016 Conf.*, Kaiserslautern, Germany **2016**.

- [150] J. Byskov-Nielsen, J. V. Boll, A. H. Holm, R. Højsholt, P. Balling, *Int. J. Adhes. Adhes.* **2010**, *30*, 485.
- [151] R. Falck, S. M. Goushegir, J. F. dos Santos, S. T. Amancio-Filho, *Mater. Lett.* **2018**, *217*, 211.
- [152] R. Falck, J. F. dos Santos, S. T. Amancio-Filho, *Materials* **2019**, *12*, 864.
- [153] A. Taub, E. De Moor, A. Luo, D. K. Matlock, J. G. Speer, U. Vaidya, *Annu. Rev. Mater. Res.* **2019**, *49*, 327.
- [154] A. Albert, W. Zorn, M. Layer, W.-G. Drossel, D. Landgrebe, L. Kroll, W. Nendel, *Technol. Lightweight Struct.* **2017**, *1*, 44.
- [155] M. Wolf, S. Hertle, D. Drummer, *Express Polym. Lett.* **2019**, *13*, 365.